NASA TN D-309

NASA TN D-309

c. 1

LOAN COPY: RETURN TO
AFSWC (STINFO)
KIRTLAND

TECH LIBRARY KAFB, NM
0152652

TECHNICAL NOTE
D-309

THE BOUNDARY-LAYER TRANSITION CHARACTERISTICS OF TWO BODIES OF REVOLUTION, A FLAT PLATE, AND AN UNSWEPT WING IN A LOW-TURBULENCE WIND TUNNEL

By Frederick W. Boltz, George C. Kenyon, and Clyde Q. Allen

Ames Research Center
Moffett Field, Calif.

NATIONAL AERONAUTICS AND SPACE ADMINISTRATION
WASHINGTON

April 1960

TECH LIBRARY KAFB, NM
0152652

NATIONAL AERONAUTICS AND SPACE ADMINISTRATION

TECHNICAL NOTE D-309

THE BOUNDARY-LAYER TRANSITION CHARACTERISTICS OF TWO BODIES OF REVOLUTION, A FLAT PLATE, AND AN UNSWEPT WING IN A LOW-TURBULENCE WIND TUNNEL

By Frederick W. Boltz, George C. Kenyon, and Clyde Q. Allen

SUMMARY

An investigation was conducted to determine the boundary-layer transition characteristics of two bodies of revolution, a flat plate, and an unswept wing. The bodies of revolution had fineness ratios of 9.0 and 7.5 and were tested at Mach numbers from about 0.1 to 0.98. The wing had an NACA 64_2A015 section and, along with the flat plate, was tested at Mach numbers below about 0.5. The beginning of transition in the boundary layer was detected with hot-wire probes and/or microphones coupled to static-pressure orifices. As a necessary part of the transition investigation, a survey of the tunnel turbulence and sound levels was also undertaken using a hot-wire anemometer and a condenser microphone.

In general, the transition Reynolds number characteristics of the several models showed similar adverse (i.e., forward movement of transition) effects of increasing tunnel airspeed in the low subsonic speed range. The pressure distribution was a primary factor in determining the level of transition Reynolds number. At low speed, however, transition Reynolds number decreased with increasing airspeed or Mach number although there were essentially no changes in the pressure distributions. It was concluded that these reductions in transition Reynolds number could be attributed to either increased air-stream turbulence or to changes in the frequency and/or intensity of sound waves with increasing airspeed. At a given tunnel airspeed or Mach number, the changes in the transition Reynolds numbers produced by changing the tunnel-drive fan blade angles and fan rotation speed provide indirect evidence that sound produced by the fan was the source of the premature transition effects.

INTRODUCTION

In recent years considerable attention has been focused on the subject of laminar-boundary-layer stability and on various means of controlling and delaying the transition from laminar to turbulent flow. Although there have been numerous tests conducted to determine the transition

Reynolds numbers on aerodynamic bodies under various conditions of stream turbulence, surface roughness, surface temperature, surface curvature, and pressure gradient, there are few data available wherein the effects of sound are clearly indicated. Perhaps the most definitive work available on the subject is that included in the classic investigation by Schubauer and Skramstad on boundary-layer stability (see ref. 1) which substantiated the Tollmien-Schlichting theory concerning the amplification of infinitesimal disturbances in the boundary layer. Included in this investigation was a study of the effects of single frequency sound waves, controlled in both frequency and intensity, on the stability characteristics of a laminar boundary layer on a flat plate. It is intended, in the present report, to show the qualitative effects of wind-tunnel noise on the boundary-layer transition characteristics of several aerodynamically smooth models when the true free-stream turbulence (vorticity) is extremely low. In addition to showing effects of natural wind-tunnel noise, it is also intended to show briefly how transition may be precipitated through the use of discrete sound waves of a given frequency introduced into the stream. All of the tests reported herein were conducted in the Ames 12-foot pressure wind tunnel.

The present investigation began with the testing of an ellipsoid of revolution of fineness ratio 9.0 to determine the subsonic effects of Mach number on the boundary-layer transition characteristics. In an attempt to gain further insight into a seemingly peculiar trend of the boundary-layer transition data for this body with increasing Mach number (a forward movement of the location of transition followed by a rearward movement), a second body of revolution of fineness ratio 7.5 was constructed and tested. This body was designed to have a more favorable pressure distribution over the forward half and thus would provide means of determining the effect of changes in the pressure gradient on the variation of the transition Reynolds number with Mach number. Although the results obtained with this body substantiated, in general, the concept that the pressure distribution was a primary factor in the stability of the boundary layer, they differed from those for the first body in a rather puzzling fashion. It was found that the rates of change of transition Reynolds number with Mach number were significantly different for the two bodies at low Mach numbers, but were similar at higher Mach numbers. Since it was thought that the explanation for the different effects was not associated with the three-dimensional nature of the flow over the bodies, it was decided to test a flat plate at several values of pressure gradient and to obtain the effect of Mach number on the values of transition Reynolds number. Further results under conditions of essentially two-dimensional flow were obtained with a wing having an NACA 64_2A015 section. In order to relate the trends found for all models to the conditions of stream turbulence, an extensive survey of tunnel-empty sound and turbulence was conducted using a condenser microphone and a hot-wire anemometer.

In the present report the data for transition Reynolds number and pressure distribution for the two bodies of revolution, the flat plate, and the wing in a low-turbulence wind tunnel are presented, as well as the level of wind-tunnel noise for the range of conditions at which transition data were obtained. A preliminary report on the boundary-layer characteristics of the two bodies of revolution at low speed ($M < 0.2$) has been presented in reference 2.

NOTATION

A	amplitude or intensity of sound wave of given frequency
A_{max}	maximum amplitude or intensity of sound wave in given sound spectrum
C_D	drag coefficient of body of revolution, $\frac{\text{drag}}{q_\infty S}$
C_p	pressure coefficient, $\frac{p_l - p_\infty}{q_\infty}$
L	length of bodies of revolution and flat plate
M	free-stream Mach number
M_n	nominal Mach number
R	length Reynolds number, $\frac{U_\infty L}{\nu}$
R_{trans}	transition Reynolds number, $\frac{U_\infty x_{tr}}{\nu}$
R_{δ^*}	Reynolds number based on boundary-layer displacement thickness, $\frac{U_\infty \delta^*}{\nu}$
S	wetted area of body of revolution
T_t	stagnation temperature
T_w	wall temperature
U_∞	free-stream velocity
b	wing span
c	wing chord

db	sound pressure level in decibels (with respect to a reference level of 0.0002 dynes per cm^2)
f	frequency, cps
p_l	local static pressure
p_t	free-stream total pressure
p_∞	free-stream static pressure
q_∞	free-stream dynamic pressure
x	axial distance along body of revolution from nose, and chord distance along flat plate and wing from leading edge
x_{tr}	x distance to location of beginning transition
y	spanwise distance from root of wing
α	angle of attack
α_n	nominal angle of attack of flat plate
β	angle of convergence between flat plate and opposite side of the channel
β_r	frequency factor ($2\pi f$) in stability parameter, $\frac{\beta_r \nu}{U_\infty^2}$
δ^*	boundary-layer displacement thickness
ν	kinematic viscosity

MODELS AND INSTRUMENTATION

Models

Four models were tested during this investigation. These were two bodies of revolution of fineness ratio 7.5 and 9.0, a flat plate, and an unswept wing having an NACA 64_2A015 airfoil section. Both bodies of revolution were sting-mounted at the center of the wind-tunnel test section. A comparative sketch of the two bodies and details of the wing and flat plate are shown in figure 1. Photographs of the models are presented in figure 2.

Bodies of revolution.- The coordinates of both bodies of revolution are listed in table I. One body was a prolate spheroid of fineness ratio 9.0, and the other body was a modified prolate spheroid of fineness ratio 7.5. The modification consisted of contouring the forward half of the body so as to provide a more favorable pressure gradient over that portion of the body. Both bodies were faired into a 4-inch-diameter sting.

The fineness-ratio-9.0 body was fabricated of 1/4-inch-thick cast-aluminum shells which were bolted together at integral internal flanges. The polished surface was estimated to have an average surface roughness of less than 30 microinches, as determined by reference to roughness gages. The surface waviness was measured with a 2-1/2-inch-span surface gage and was found to be less than 0.0003 inch per inch.

The fineness-ratio-7.5 body was constructed of steel shells welded together around a core of steel tubing. The body was covered with a 1/4-inch layer of Fiberglas and resin which, in turn, was coated with a 1/32-inch layer of epoxyresin. The resin surface was sprayed with several coats of hard lacquer and was hand-rubbed with number 600 sandpaper to a smooth finish. The surface roughness was comparable to that of the aluminum body. The surface waviness was found to be less than 0.0004 inch per inch as measured with a 2-1/2-inch-span surface gage.

Flat plate.- The flat plate consisted of a 1/2-inch-thick rectangular aluminum plate on which elliptical contours were machined to form the leading and trailing edges. The leading-edge profile was that of a 24-to-1 ellipse so that the flat surface began 6 inches from the leading edge. The working surface of the plate was polished to a mirrorlike finish with a roughness comparable to that of the bodies of revolution. The surface waviness was found to be less than 0.0004 inch per inch as measured with a 2-1/2-inch-span surface gage. As shown in figure 1, the flat plate was mounted on the supporting structure so that it formed one wall of a closed channel. The entire assembly was mounted on a turntable in the floor of the wind-tunnel test section, which permitted variation of the angle of attack. The pressure distribution along the surface of the flat plate was controlled by changing both the angle of attack and the angle between the flat plate and the opposite wall of the channel.

Wing.- The unswept wing was constructed entirely of steel and was mounted on the turntable in the floor of the test section as shown in figure 1. The model had a constant chord of 4 feet and a span of 10 feet. Coordinates of the NACA 64_2A015 airfoil section are listed in table II. The surface of the wing was formed by 3/8-inch-thick steel plates rolled to the approximate contour, welded to three channel-beam spars, and machined to the final shape. The final surface finish was obtained by sanding with number 400 sandpaper. The surface waviness was found to be less than 0.0005 inch per inch as measured with a 2-1/2-inch-span surface gage. The tip of the wing was formed by a half-body of molded Fiberglas and resin having radii corresponding to the airfoil coordinates.

Instrumentation

Stream measurements.- Measurements of the turbulence level of the air stream were made with a hot-wire anemometer developed at the Ames Research Center. The anemometer is a constant-current type having a compensating amplifier. The hot-wire elements were tungsten with a diameter of 0.00015 inch and a length of approximately 0.105 inch.

Measurements of the sound pressure level in the wind-tunnel test section were obtained with an Altec-Lansing model No. 21 BR-180 condenser microphone in conjunction with its P 526A power supply. A vacuum-tube voltmeter was used to measure the microphone output signal which was amplified and recorded on magnetic tape. The microphone was centrally mounted in the wind-tunnel test section in two different configurations. These configurations, illustrated in figure 3, were obtained by fitting the microphone into two small bodies of revolution. The bodies were sting-mounted and located along the center line of the wind tunnel but the microphone was 10 inches farther forward in one body than in the other

In order to introduce sound of controlled frequency and intensity into the test section, eight 25-watt speakers were placed in the wind-tunnel settling chamber upstream from the test section. A variable-frequency oscillator connected to the speakers through audio amplifiers furnished known frequencies for the test. Magnetic tape recordings of tunnel noise were played back into the tunnel through the speakers to intensify the natural tunnel noise at any particular operating condition. Frequency analyses of the tape recordings to determine the frequency spectrum of the tunnel noise were obtained using a wave analyzer coupled to a Brown recorder.

Model instrumentation.- The four models tested were instrumented to obtain static-pressure-distribution and boundary-layer-transition data. Pressure distributions were measured on multiple-tube manometers and were recorded photographically. Transition detection was accomplished with surface-mounted hot-wire probes (see fig. 4(c)) and with small microphones located in the models and closely coupled to static-pressure orifices (as illustrated in figs. 4(a) and 4(b)). The probes consisted of 0.0003-inch-diameter tungsten wire, approximately 0.11 inch in length, which was spot-welded to the conical tips of two 1/16-inch-diameter needles. The needles were embedded in a plastic body which held them rigid and parallel. The microphones were actually small magnetic-type receivers (U. S. Signal Corps Headset H.S.-30-V). The output signal from each type of sensing device was amplified and passed through a band-pass filter to a headset receiver and an oscilloscope, permitting the signal to be interpreted both audibly and visually. In figure 5 is shown a photographic record of an oscilloscope trace of the microphone response to three types of boundary-layer flow. It should be noted that in each of the three traces there is a common waviness due to the internal "noise" of the electrical equipment.

The locations of the static-pressure orifices and subsurface microphones for both bodies of revolution are given in table III. Also listed are the locations of 11 thermocouples embedded just beneath the epoxyresin surface of the fineness-ratio-7.5 body. The temperatures detected by the thermocouples were recorded by a multiple-channel Brown recorder. Transition data for the fineness-ratio-7.5 body were also obtained by means of a hot-wire probe taped to the surface at the 60-percent-length station. Skin-friction drag data for both bodies were obtained with boundary-layer survey rakes of static- and total-pressure tubes installed at the 100-percent-length station of the models as shown in figure 2(d).

The flat plate was equipped with a row of static-pressure orifices as shown in figure 1 and listed in table IV. Microphones were connected in the manner shown in figure 4(b) to a row of surface orifices near the center line of the plate. The exact location of these microphone orifices is also indicated in table IV. A hot-wire probe was cemented to the plate surface at the 60-percent-length station.

The wing was equipped with two rows of static-pressure orifices as shown in figure 1 and listed in table V. Six hot-wire probes were cemented to the wing surface at the 20-, 25-, 30-, 35-, 40-, and 45-percent-chord stations.

TESTS

The tests made during this investigation were conducted in the Ames 12-foot pressure wind tunnel. Free-stream sound and turbulence measurements with the wind tunnel empty were obtained for the entire operating range of pressure and velocity.

The two bodies of revolution were tested at zero angle of attack. During these tests, the unit Reynolds number was maintained at several constant values by varying the tunnel pressure for the different Mach numbers. For both bodies, pressure measurements along the surface and in the wake (around the sting) were made simultaneously with locating the point of beginning transition for Mach numbers from about 0.1 to 0.98.

The flat plate was tested at nominal angles of attack from -2° to $+1^\circ$ with the convergence angle of the channel set at -0.18°, 0°, and $+0.6^\circ$. (The geometric angle of attack of the plate can be obtained by subtracting the convergence angle from the nominal angle of attack.) Transition data were obtained by increasing the Mach number at a given pressure until the location of beginning transition was at the hot-wire station or at successive microphone stations.

The wing was tested at angles of attack from -3° to $+3^{\circ}$. As in the case of the flat plate, the transition data were obtained by increasing the Mach number at a given pressure until the point of beginning transition was at successive detection stations.

CORRECTIONS TO DATA

Blockage corrections for both bodies of revolution and the wing were computed according to the method of reference 3 and have been applied to the data. The magnitudes of the corrections applied to the free-stream Mach number for each model are illustrated in the following tables:

Fineness-ratio-7.5 body		Fineness-ratio-9.0 body	
Corrected Mach number	Uncorrected Mach number	Corrected Mach number	Uncorrected Mach number
0.10	0.100	0.10	0.100
.50	.497	.50	.498
.60	.496	.60	.497
.70	.694	.70	.696
.80	.788	.80	.792
.90	.872	.90	.880
.98	.921	.98	.932

Wing	
Corrected Mach number	Uncorrected Mach number
0.10	0.099
.20	.197
.30	.295
.40	.392
.50	.489

All of the flat-plate data, including the values of pressure coefficient, are presented in terms of free-stream values uncorrected for blockage effects.

RESULTS AND DISCUSSION

The stability of the laminar boundary layer on an aerodynamically smooth body is affected by many factors including the mean static-pressure gradient and the fluctuations or turbulence in the external flow. For tests conducted in a wind tunnel, there can often be a finite pressure gradient imposed on the natural gradient of a model at high speeds which may produce transition results considerably different from those in free air. In similar fashion, the effects of wind-tunnel turbulence and of

changes in turbulence with speed may produce results different from those obtained in free air. Since these effects were of major importance in the present investigation, they will be discussed briefly before the presentation and discussion of the boundary-layer transition results.

Wind-Tunnel Flow Conditions

Test-section pressure gradient.- The variation of the static-pressure gradient through the test section with the tunnel empty (no model in the test section) has been obtained for the entire test range of subsonic Mach numbers and is presented in figure 6. It can be seen that the gradient is insignificant for Mach numbers less than 0.60, but becomes quite favorable for delaying transition at higher Mach numbers. The longitudinal positions of three of the models in the test section are also indicated in figure 6 by their position relative to the pressure distributions. The flat-plate position is not indicated in figure 6, since it was tested in a closed channel in the test section and, therefore, the indicated pressure distributions do not apply. It should be noted that the blockage effects with the models in the test section would cause the effective flow fields and pressure gradients to be different from those found with the tunnel empty.

Free-stream turbulence level.- As indicated in reference 4, the turbulence flow field in a wind tunnel may be divided into three modes: vorticity mode, entropy mode, and sound-wave mode. The vorticity mode represents the turbulent velocity fluctuations (eddying motion) found in wakes and in turbulent boundary layers, while the entropy mode represents the nonisentropic temperature variations in the stream. The sound-wave mode represents the irrotational velocity fluctuations and the isentropic pressure, density, and temperature fluctuations in the stream. In a low-turbulence wind tunnel, such as the Ames 12-foot pressure tunnel, the vorticity and entropy modes are generally of very low intensity. At low speeds the sound-wave mode is also generally very weak. However, at higher speeds the intensity of the sound waves may attain extremely high values. At all subsonic speeds the sound field consists of sound waves randomly oriented at any given location in the stream but generally moving upstream or downstream.

In figure 7, the results of sound-pressure-level measurements in the test section of the 12-foot tunnel are presented.[1] The decibel level indicated is with respect to a reference pressure amplitude of 0.0002 dynes per square centimeter. An Altec condenser microphone, mounted in two different ways (see fig. 3) near the center line of the test section, was used to detect the pressure fluctuations. Because of the smaller effects

[1]It should be noted that, in figure 7 and in other figures in the report, the pair of blade angles indicated has reference to the upstream and downstream stages of the two-stage tunnel-drive fan.

of flow-field disturbance resulting from the use of a microphone mounting in a body with a higher critical speed (as discussed below), it is believed that the set of data obtained with the microphone mounted in the static-orifice arrangement is the more representative of the average sound pressure level in the test section at all Mach numbers. Although it is not indicated in the data of figure 7, the results of the sound survey disclosed that the sound pressure level in the tunnel, at a given condition of Mach number and pressure, increased when the blade angles of the tunnel-drive fan were reduced and the rotational speed was consequently increased. This effect is later shown to have had an influence on the transition Reynolds numbers obtained for the various models. From a consideration of both sets of data, it would appear that the most intense sound waves at the higher Mach numbers are those moving in the upstream direction. This conclusion is based on: (1) the leveling off of the curves in figure 7(a) at Mach numbers above the critical speed ($M \cong 0.5$) of the blunt body (stagnation-point microphone mounting), and (2) the sudden loss of sound pressure level in the data of figure 7(b) at Mach numbers above the critical speed ($M \cong 0.9$) of the pointed body (static-orifice microphone mounting) and where the wind-tunnel test section was nominally choked. Since upstream-moving sound waves cannot penetrate sonic or supersonic flow, the only response of the microphone under these conditions is to sound waves moving downstream.

If the sound waves are assumed to be plane and moving in one direction, the root-mean-square particle velocities can be calculated from the given sound pressure levels in decibels by means of the expression

$$\frac{\Delta U}{U} = \frac{10^{0.05\ \mathrm{db} - 3.7}}{\gamma M p}$$

where p is the local mean static pressure in dynes per square centimeter. For instance, at atmospheric pressure ($p = 10^6$ dynes/cm^2) and at a Mach number of 0.1, the value of longitudinal velocity fluctuation $\Delta U/U$ is 0.0143 percent for 100 db. At a stagnation pressure of 1/3 atmospheric pressure and at a Mach number of 0.9, the value of $\Delta U/U$ is 0.637 percent for 138 db. Thus, it is seen that rather large velocity fluctuations may accompany the intense pressure and density fluctuations at the higher Mach numbers.

In order to be sure that there were no turbulent velocity fluctuations (vorticity mode) of greater magnitude than those indicated from the sound measurements, turbulence measurements were made with a hot-wire anemometer throughout the subsonic range of Mach numbers. The intensities of all three modes of turbulence at low speeds were apparently too low to be resolved accurately through the use of present hot-wire equipment. In the case of the vorticity mode, however, it was indicated that the turbulent velocity fluctuations, $\Delta U/U$, were probably of the order of about 0.0002 or less. The analysis indicated further that sound waves could account for practically all of the intense fluctuations measured with the hot-wire anemometer at the higher Mach numbers. This result suggests that

even at high speed in the 12-foot pressure tunnel the intensity of turbulent velocity fluctuations is relatively low. It should be noted, however, that, because of the high level of sound-wave intensity at the higher Mach numbers and the complexity of the sound field consisting of sound waves moving both upstream and downstream, it was not possible to obtain an estimate of the increase, if any, in the level of turbulent velocity fluctuations from their probable low-speed level.

Frequency analysis of sound.- In addition to the increase in the intensity of the sound waves with increasing Mach number, there was found to be a change in the frequency of the sound relative to a fixed point in the flow. The frequencies of vibration present in the sound field are believed to be significant because of the mechanism of selective amplification of disturbances of certain frequencies in the boundary layer as presented in the Tollmien-Schlichting theory. It is suggested later that the absence of sound waves of sufficiently high frequency may account, in part, for the comparatively high values of transition Reynolds number found for the bodies of revolution at the higher Mach numbers. In order to determine the frequency content of the sound, a frequency analysis was made of taped recordings of the microphone signal. The results of this analysis for a wide range of subsonic Mach numbers are presented in figure 8. These data were obtained at essentially constant stagnation density with the stream Reynolds number per foot varying from about 0.15×10^6 to about 0.80×10^6 and have been normalized with respect to the maximum output amplitude from the analyzer. It is understood, therefore, that no quantitative comparison of absolute amplitude can be made for the different Mach numbers. The tapered and flared appearance of the response curves is due in part to the filter characteristics of the analyzer and to fluctuations in the actual frequencies of the waves with time.

It is apparent from these frequency spectra that, in general, the major part of the sound field at all subsonic Mach numbers is composed of waves having frequencies less than 600 cycles per second relative to a fixed point in the test section. Furthermore, it appears that there is no direct relation between the predominant frequencies present in the sound field and the tunnel Mach number. It is more likely that the frequencies are related, in most cases, to the speed of rotation of the tunnel fan, since different frequency spectra were obtained at a given Mach number by changing the fan blade angles and, consequently, the fan speed. However, for constant fan blade angles, the frequency spectrum at a given Mach number was found to be essentially independent of the tunnel pressure. For all of the data shown in figure 8, which were obtained for various Mach numbers at a constant value of stagnation pressure, the fan blade angle was also constant.

Pressure-Distribution and Boundary-Layer-Transition Results

Bodies of revolution.- The pressure distributions measured on the two bodies of revolution at various subsonic speeds are presented in figures 9 and 10. A comparison of the experimental pressure distributions for the fineness-ratio-9.0 body at Mach numbers of 0.25 and 0.90 with those obtained from theory is presented in figure 9(a). The low-speed theoretical values were calculated according to the method of reference 5 for incompressible potential flow, and these values were modified according to the method given in reference 6 to obtain the high-speed values. In the case of the fineness-ratio-7.5 body, which was not derived from a simple mathematical expression (ellipsoid for the fineness-ratio-9.0 body), the calculative procedure was considerably more complicated and theoretical pressure distributions were not obtained. However, a comparison of the experimental pressure distributions for both bodies at low speed and at high speed is presented in figure 9(b). The progressive changes in the measured pressure distributions for both bodies with increasing Mach number are presented in figure 10.

It is apparent that rather large differences in pressure gradient existed between the two bodies at all Mach numbers. With increasing Mach number the pressure gradients became more negative over the forward portions of both bodies and the pressure coefficients at the minimum pressure points were reduced slightly. It should be noted that the degree of the change in pressure gradient over the forward portions of the fineness-ratio-9.0 body is greater than predicted by potential-flow theory by an amount which is attributable to effects of tunnel blockage and tunnel pressure gradient.

The results of measurements of the location of boundary-layer transition and of the wake drag for both bodies of revolution at several Reynolds numbers are presented in figure 11. The wake-drag measurements were made to confirm the seemingly peculiar trend of the boundary-layer-transition data with increasing Mach number. Although not indicated in figure 11, there was found to be good agreement between the locations of transition measured with the microphone-detection method and the locations of transition calculated from the wake-drag results in conjunction with the well-known expressions for laminar and turbulent skin-friction coefficient.

From figure 11 it is seen that there were large differences in the location of transition on the bodies at corresponding Reynolds numbers for all except the highest and lowest Mach numbers. The rearward movement of transition for both bodies at the higher Mach numbers is believed to have been due to the increase in the favorable pressure gradients over the forward portions of the bodies and to the absence of sound waves of a critical frequency. (According to the Tollmien-Schlichting stability theory as discussed in reference 1, the values of critical frequency are

proportional to the velocity or Mach number and, therefore, are greatly increased over their low-speed values at high Mach numbers.) The differences in the rate of change of the values of transition Reynolds number for the two bodies at low Mach numbers indicate a difference in the boundary-layer stability characteristics and are believed to have resulted from the differences in the pressure gradients at corresponding points on the bodies.

Perhaps a brief discussion of the mechanism believed to be in operation between the boundary layer and sound waves present in the flow field would be helpful in understanding some of the trends in the data alluded to above. With reference again to figure 7, it is seen that there was generally an increase in the intensity of the tunnel noise with increasing Mach number at all pressures. This noise was composed of superimposed sound waves of many frequencies which changed with the Mach number. The manner in which small periodic disturbances, such as sound waves, may be greatly amplified in a laminar boundary layer with the result of a transition to turbulent flow has been studied in detail in reference 1. It is believed that there is a critical disturbing frequency which results in the greatest amount of amplification of a disturbance for any set of given conditions of mean flow velocity, pressure distribution, and location on the surface. For disturbances of slightly different frequency, the total amplification to the particular location being considered would not be as great. It is, of course, apparent that the amplitude of the disturbing influence, such as fluctuations caused by a sound wave, is also of major importance in the eventual breakdown of laminar motion. The differences in the amplification rates of boundary-layer fluctuations in various pressure gradients is only qualitatively known (according to the Tollmien-Schlichting theory), but it is believed to be the reason for certain otherwise anomalous results which have been obtained.

The transition data for the fineness-ratio-7.5 body in figure 11 are presented in a slightly different manner in figure 12, along with other data obtained for the condition when the location of transition was always at 60 percent of the body length. These two sets of data were obtained in different tests and with different transition-detection techniques which may be responsible for slight inconsistencies in the results. It is seen that slightly higher values of transition Reynolds number were obtained at low Mach numbers with a constant location of transition than were obtained with constant values of length Reynolds number (Reynolds number based on body length). It is to be noted that the length Reynolds numbers of the data shown with constant location of transition at $x/L = 0.60$ were between about 6.0×10^6 and 8.5×10^6. The reason for the apparent small discrepancy at very low speed between the data for constant transition location and the data for constant length Reynolds number is not definitely known. The accuracy of the data at very low Mach number may be a factor in the different trends indicated, since small variations, of the order of 1 pound per square foot, in the dynamic pressure could produce substantial changes in the Mach number and Reynolds number.

As noted in the description of the instrumentation of the models, the fineness-ratio-7.5 body was equipped with a lengthwise row of thermocouples for measuring the surface temperatures. These thermocouples provided a check at the higher Mach numbers on the accuracy of transition location as detected with the microphones coupled to the static-pressure orifices. Representative temperature distributions obtained along the length of the body at several Mach numbers are presented in figure 13. Transition was considered to begin at the station corresponding to the minimum point of each curve. The results obtained by this means of detection were found to be in excellent agreement with those obtained with the internally located microphones and the surface-mounted hot-wire probes.

Flat plate.- The transition Reynolds numbers and the static-pressure distributions obtained with the flat plate are presented in figures 14 and 15. Different pressure distributions were obtained by varying the angle between the flat plate and the opposite side of the channel as well as the angle of attack of the entire assembly. For the data of figure 14, transition was detected with a hot wire at 60 percent of the plate length. It is quite apparent from these results that small variations in the pressure distribution on a flat plate can cause rather large variations in the values of transition Reynolds number.

To cover the available range of Reynolds numbers and Mach numbers in the Ames 12-foot pressure wind tunnel it is necessary to change the blade angle of the tunnel drive fan. As was mentioned earlier, the sound pressure level in the tunnel at a given condition of Mach number and pressure increased when the blade angles were reduced and the rotational speed of the fan was increased. It is indicated from the data of figure 14 that the value of transition Reynolds number was slightly dependent on the fan blade angles for a given Mach number and angle of attack. The degree of this dependence is seen to have been affected by the pressure distribution.

It is to be noted that the fairing of the transition data in figure 14 is only nominal. It is believed that the apparent "scatter" in the data is more likely a result of variations with Mach number in both the intensity and frequency of the sound waves present in the stream as well as of a variation in the boundary-layer stability limits. The actual variation of the transition Reynolds numbers with Mach number could not then be expected to follow a smooth curve.

The effect of varying the location of transition on the transition Reynolds number for a constant angle between the channel plates and a constant angle of attack is shown in figure 15. For these results transition was detected with several microphones between 50 and 90 percent of the plate length. The data were obtained by operating at several different values of stagnation pressure in the tunnel and increasing the speed at each pressure until the point of transition had progressed from the

rearmost to the foremost measuring station on the flat plate. The effect to be noted here is that a different level of similar variation of transition Reynolds number with Mach number was obtained for each of the various transition-detecting stations on the plate. This is compatible with the results shown on figure 14.

Wing.- The data for transition Reynolds number and the static-pressure distributions for the wing are presented in figures 16 and 17, respectively. The data of figure 16 were obtained with hot-wire probes for several angles of attack and for several chordwise positions of transition on the wing. The corresponding pressure-distribution data of figure 17 were measured on either side of the middle area of the wing where the values of transition Reynolds number were determined (see fig. 1).

It is apparent from a comparison of figures 14 and 16 that, in general, the boundary layer on the wing reacted to the changing flow conditions in a manner similar to that of the boundary layer on the flat plate. There was found to be a slight reduction in the transition Reynolds number with increasing Mach number as well as a sudden change in the transition Reynolds numbers due to a change in tunnel-drive fan blade angle. No explanation is apparent for the reduction in transition Reynolds number at the lowest velocities.

Sound-Augmentation Tests

In order to obtain more definite evidence of the effects of sound in causing earlier transition, a brief test of the flat plate was undertaken in which the natural tunnel sound was augmented by sound introduced into the stream by means of eight 25-watt loudspeakers. The loudspeakers were located on the floor of the tunnel settling chamber and directed so as to create sound waves moving approximately parallel to the lower wall of the entrance nozzle to the test section. The first part of the tests consisted of recording the natural tunnel noise at a given condition and then playing back this sound through the loudspeakers at their rated capacity. The results are shown in figure 18. It should be mentioned that the pressure distribution on the flat plate was approximately as shown in figure 14(a) ($\alpha_n = -1^\circ$).

The final part of the tests consisted of introducing sound of a single frequency into the stream via the loudspeaker system and an audio oscillator. Various frequencies were introduced at a given Mach number and it was found that at each tunnel pressure a particular frequency was most effective in moving transition forward. The data in figure 18 show the large effects of the single frequencies on transition Reynolds numbers. This result was to be expected, of course, in consideration of the Tollmien-Schlichting theory (see ref. 7).

As a matter of interest, the location on the boundary-layer stability diagram (for a flat plate with zero pressure gradient) of the experimental single-frequency data for beginning transition is also shown in figure 18. The values of $R\delta^*$ were obtained from calculated values of the displacement thickness of the boundary layer and the free-stream value of velocity. According to theory, the amplification of a disturbance should be a maximum for points on the upper branch of the neutral stability curve in this diagram. It is seen that the present data are in better agreement with the more recent computation of the neutral stability curve given in reference 8 than with that given by Schlichting in reference 7.

In order to determine the amount of energy introduced into the stream by the loudspeakers operating at rated capacity, the sound pressure level in the test section was measured with the loudspeakers operating and the tunnel not running. It was found that the decibel level was essentially constant at 115 db for a broad range of input frequency and was the same for tunnel noise played back as for single-frequency sound.

SUMMARY OF RESULTS

The results of an investigation of the boundary-layer transition characteristics of two bodies of revolution, a flat plate, and an unswept wing in a low-turbulence wind tunnel and of a survey of the tunnel turbulence and sound levels may be summarized as follows:

1. In all cases it was found that the pressure distribution on the model was a primary factor in determining the level of transition Reynolds number. Small increases in the favorable pressure gradients over the forward portion of the models resulted in significant increases in the transition Reynolds number.

2. Measurements of the tunnel turbulence and sound pressure levels with a hot-wire microphone and a condenser microphone indicate that sound comprises practically the entire "turbulence" field at all Mach numbers. The so-called "true" turbulence or vorticity present in the stream is believed to be extremely low ($\Delta U/U$ the order of about 0.0002 or lower) and below a resolvable level with usual turbulence-measuring equipment. In general, increasing the airspeed in the tunnel results in an increase in both the intensity and frequency content of sound waves. Increasing the tunnel pressure at a given Mach number also results in an increase in the intensity of sound waves, although there is essentially no change in the frequency content as long as the rotation speed of the tunnel drive fan remains constant. At the higher Mach numbers the maximum frequency of sound waves is probably well below the critical values for boundary-layer instability as given by the Tollmien-Schlichting theory.

3. In general, it was found that increasing tunnel airspeed had an adverse effect on the transition Reynolds numbers for all of the models in the low subsonic speed range. It is believed that the effect was a result of changes in the frequency and/or intensity of the sound waves present in the flow field.

Ames Research Center
National Aeronautics and Space Administration
Moffett Field, Calif., Dec. 14, 1959

REFERENCES

1. Schubauer, G. B., and Skramstad, H. K.: Laminar-Boundary-Layer Oscillations and Transition on a Flat Plate. NACA Rep. 909, 1948.

2. Boltz, Frederick W., Kenyon, George C., and Allen, Clyde Q.: Measurements of Boundary-Layer Transition at Low Speed on Two Bodies of Revolution in a Low Turbulence Wind Tunnel. NACA RM A56G17, 1956.

3. Herriot, John G.: Blockage Corrections for Three-Dimensional-Flow Closed-Throat Wind Tunnels, with Consideration of the Effect of Compressibility. NACA Rep. 995, 1950.

4. Kovasznay, Leslie S. G.: Turbulence in Supersonic Flow. Jour. Aero. Sci., vol. 20, no. 10, Oct. 1953, pp. 657-674, 682.

5. Zahm, A. F.: Flow and Drag Formulas for Simple Quadrics. NACA Rep. 253, 1927.

6. Matthews, Clarence W.: A Comparison of the Experimental Subsonic Pressure Distributions About Several Bodies of Revolution With Pressure Distributions Computed by Means of the Linearized Theory. NACA Rep. 1155, 1953.

7. Schlichting, Hermann: Boundary Layer Theory. McGraw-Hill Book Co., Inc. First Eng. ed., 1955.

8. Timman, R., Zaat, J. A., and Burgerhout, T. J.: Stability Diagrams for Laminar Boundary Layer Flow. NLL-TN F. 193 (1956).

TABLE I.- BODY OF REVOLUTION COORDINATES
[All dimensions given in percent length]

Fineness-ratio-9.0 body				Fineness-ratio-7.5 body			
Station	Ordinate	Station	Ordinate	Station	Ordinate	Station	Ordinate
0	0	30.0	5.03	0	0	30.0	6.02
.5	.77	34.0	5.24	.5	.95	35.0	6.31
1.0	1.09	40.0	5.37	1.0	1.29	40.0	6.51
2.0	1.54	45.0	5.45	2.0	1.75	45.0	6.63
3.0	1.87	50.0	5.47	3.0	2.09	50.0	6.67
4.0	2.16	55.0	5.43	4.0	2.38	55.0	6.63
5.0	2.41	60.0	5.33	5.0	2.64	60.0	6.53
6.0	2.61	65.0	5.18	6.0	2.88	65.0	6.36
7.0	2.81	70.0	4.96	7.0	3.10	70.0	6.11
8.0	2.99	75.0	4.67	8.0	3.30	75.0	5.77
9.0	3.15	80.0	4.26	9.0	3.49	80.0	5.33
10.0	3.30	85.0	3.76	10.0	3.67	85.0	4.76
15.0	3.94	89.0	3.06	15.0	4.46	90.0	4.00
20.0	4.41	95.0	2.01	20.0	5.10	95.0	2.91
25.0	4.76	100.0	2.00	25.0	5.62	100.0	2.08

TABLE II.- COORDINATES FOR THE NACA 64_2A015 WING
[All dimensions given in percent chord]

Station	Ordinate	Station	Ordinate
0	0	40.00	7.487
.50	1.193	50.00	6.978
.75	1.436	55.00	6.517
1.25	1.815	60.00	5.956
2.50	2.508	65.00	5.311
5.00	3.477	70.00	4.600
7.50	4.202	75.00	3.847
10.00	4.799	80.00	3.084
15.00	5.732	85.00	2.321
20.00	6.423	90.00	1.558
25.00	6.926	95.00	.795
30.00	7.270	100.00	.032
35.00	7.463		

Leading-edge radius: 1.561 percent c
Trailing-edge radius: 0.037 percent c

TABLE III.- STATIC-PRESSURE ORIFICE, MICROPHONE, AND THERMOCOUPLE LOCATIONS FOR BODIES OF REVOLUTION

[All dimensions given in percent length]

Fineness-ratio-9.0 body	Fineness-ratio-7.5 body
Upper surface meridian	Upper surface meridian
Station	Station
5.8	0
11.5	.20
20.8	.59
28.6^{m}	1.50^{t}
34.4^{m}	2.95
45.3^{m}	4.80
54.2^{m}	7.10
63.5^{m}	9.95^{mt}
70.8^{m}	15.00^{m}
77.1^{m}	20.00^{mt}
81.8^{m}	24.92^{m}
85.9^{m}	30.00^{mt}
91.7^{m}	35.00^{m}
95.8	40.00^{mt}
	45.00^{m}
	49.98^{mt}
	55.00^{m}
	60.00^{mt}
	65.00^{m}
	70.00^{mt}
	75.00^{m}
	80.00^{mt}
	85.00^{m}
	90.00^{mt}
	100.00^{+}

Note: m denotes microphone at orifice station
t denotes thermocouple locations
+ denotes 100 percent length for thermocouple only

TABLE IV.- STATIC-PRESSURE ORIFICE AND MICROPHONE ORIFICE LOCATIONS FOR FLAT PLATE

[All dimensions given in percent length measured from leading edge]

Pressure orifice station[a]	Microphone orifice station[b]
0	10.18
.22	15.21
2.93	20.23
4.56	25.26
6.16	30.28
9.48	35.31
14.42	40.33
19.38	45.36
24.32	50.39
29.28	55.41
34.22	60.44
39.18	65.46
44.12	70.49
49.08	75.51
54.02	80.54
58.96	85.56
63.92	90.59
68.86	
73.82	
78.76	
83.72	
88.66	
93.68	

[a]Aligned 10° to stream direction

[b]Along center line of flat plate in stream direction

TABLE V.- STATIC-PRESSURE ORIFICES FOR 64_2A015 WING

[Orifices located at 45- and 80-percent spanwise stations. All dimensions given in percent chord.]

Station	Station
0	44.8
1.4	49.9
4.1	54.9
7.0	59.9
10.1	65.0
15.9	69.0
20.8	75.0
23.9	80.0
29.9	85.0
34.8	89.0
39.8	94.8

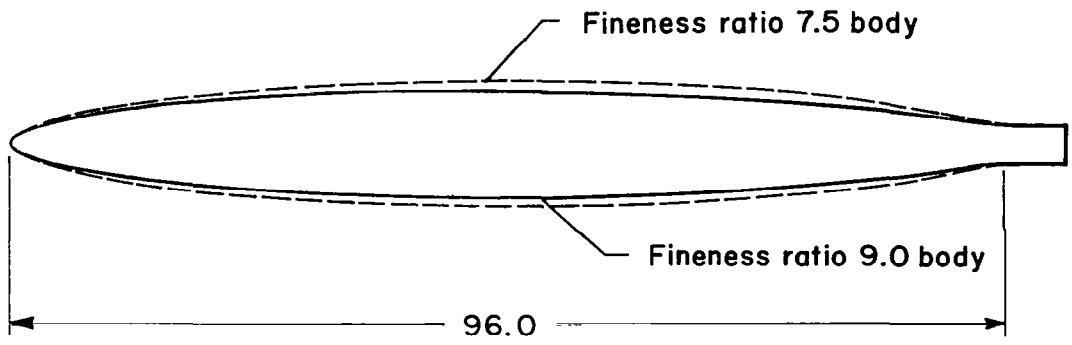

(a) Two bodies of revolution.

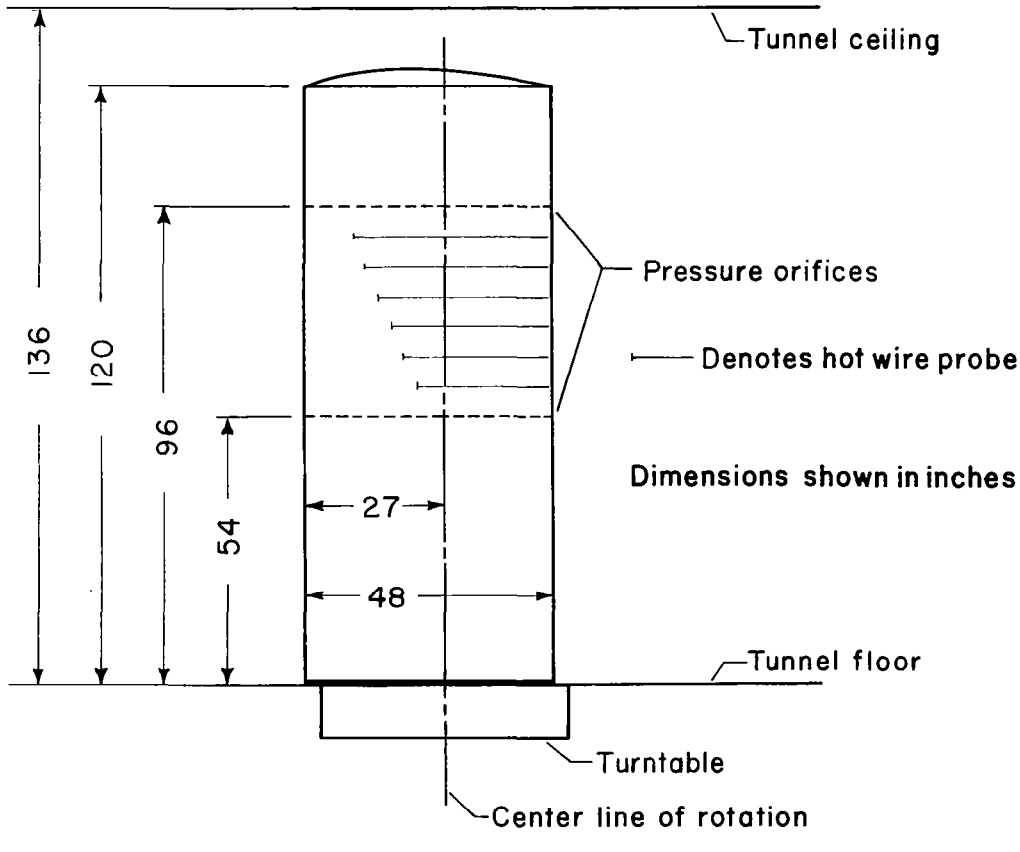

(b) Wing.

Figure 1.- The four models tested in the investigation.

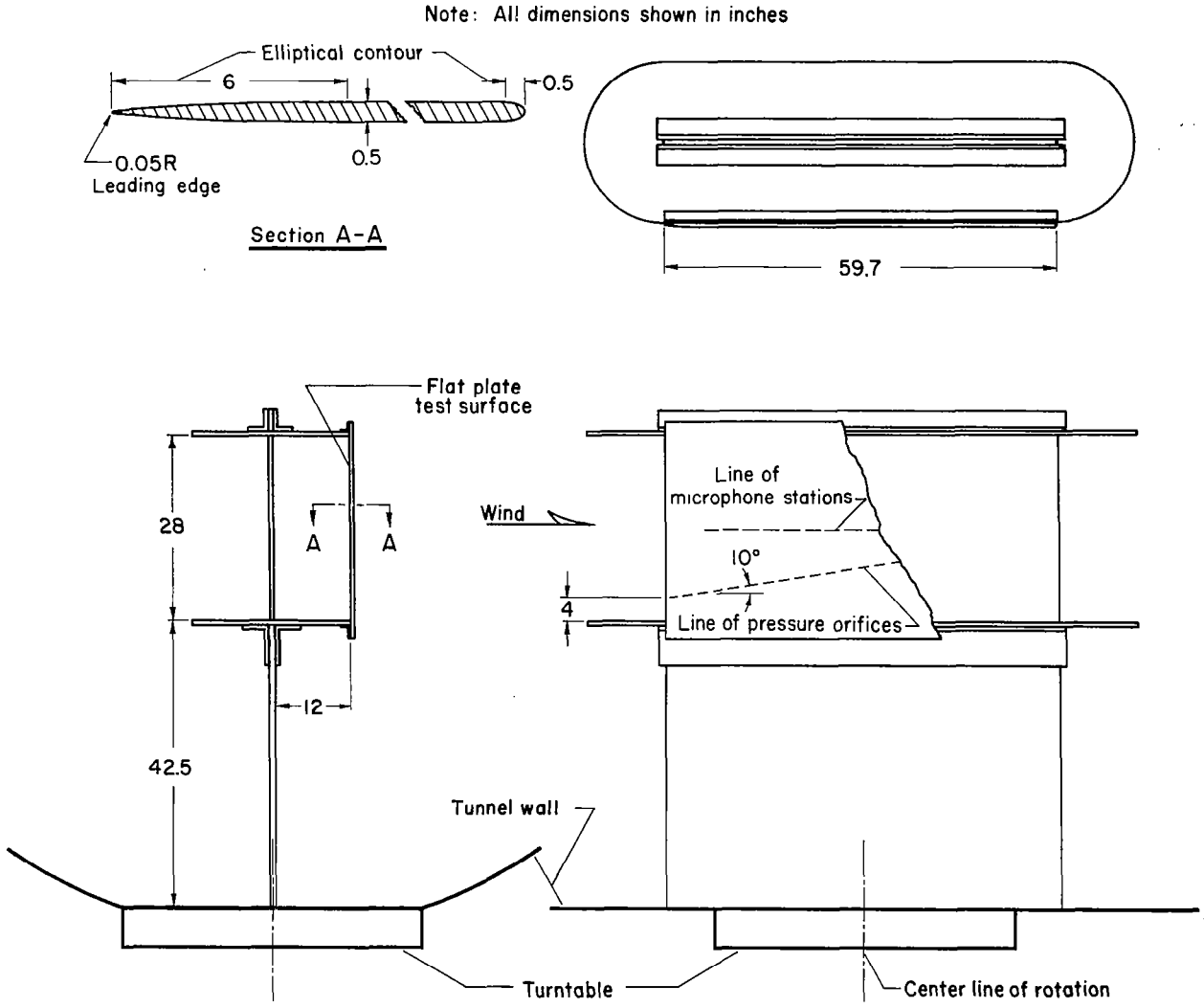

(c) The flat plate and supporting structure.

Figure 1.- Concluded.

(a) The body of fineness ratio 9.0. A-19928

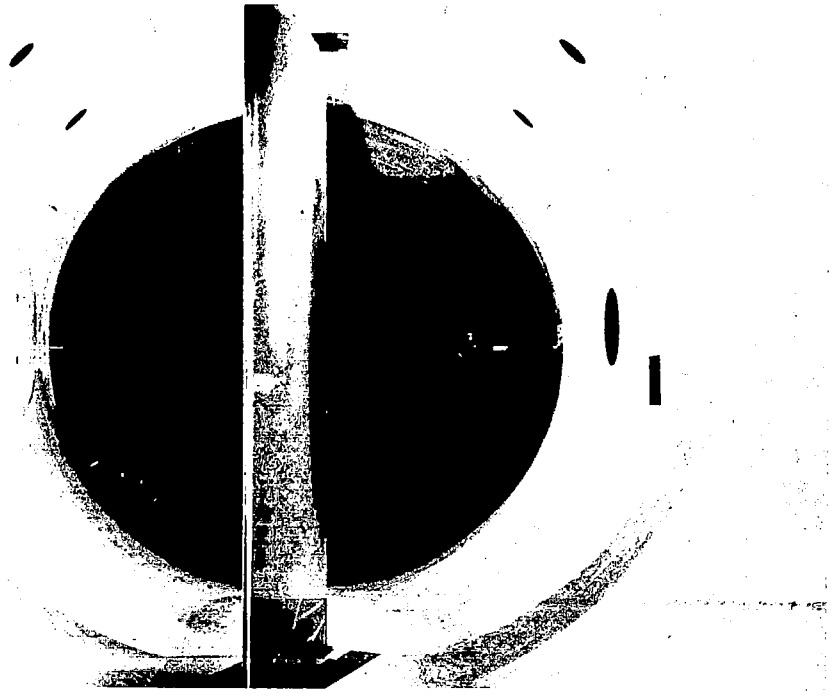

(b) The unswept wing. A-25580

Figure 2.- Photographs of the models in the wind tunnel.

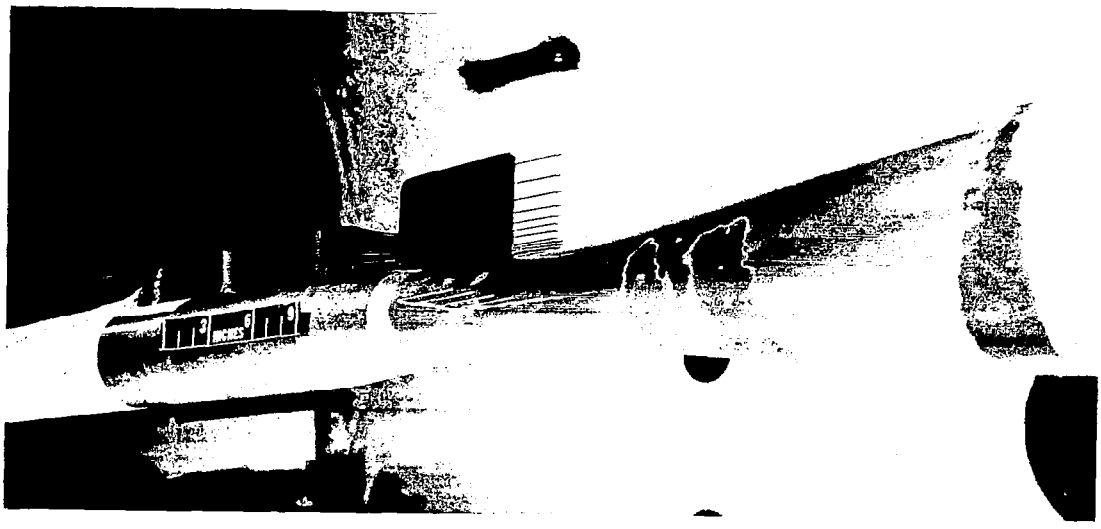

(c) The wake-drag survey rake. A-19929

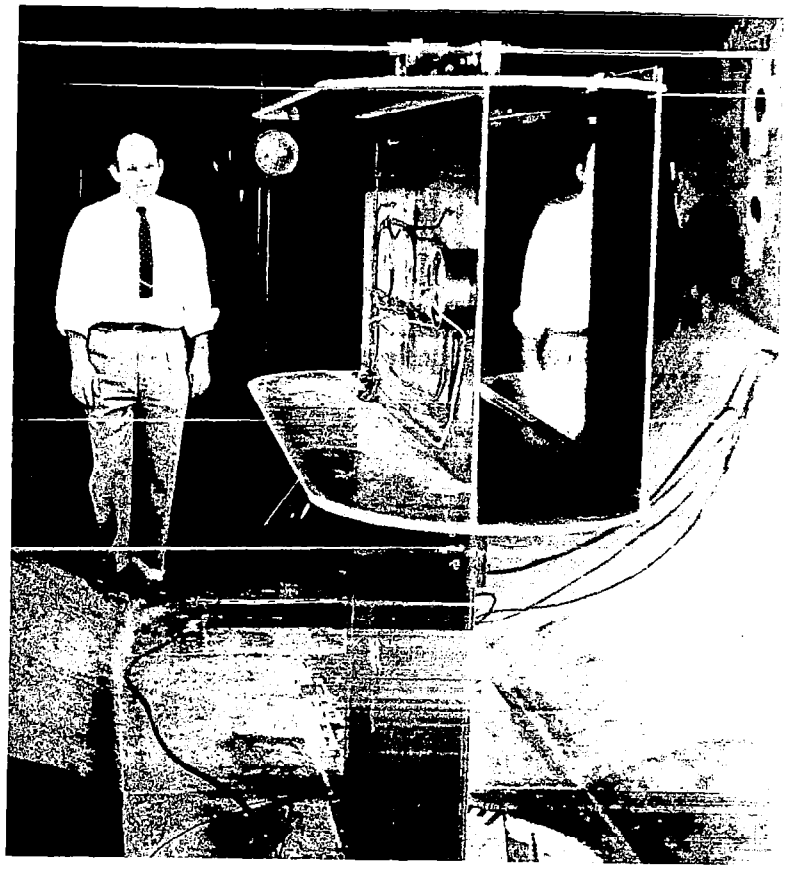

A-20561

(d) The flat plate and supporting structure.

Figure 2.- Concluded.

ALL DIMENSIONS SHOWN IN INCHES

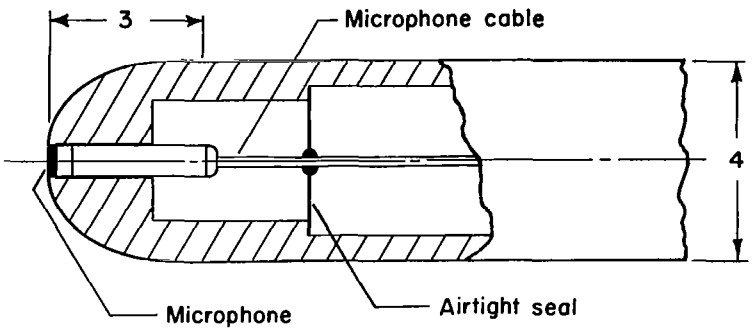

(a) Stagnation-point microphone mounting.

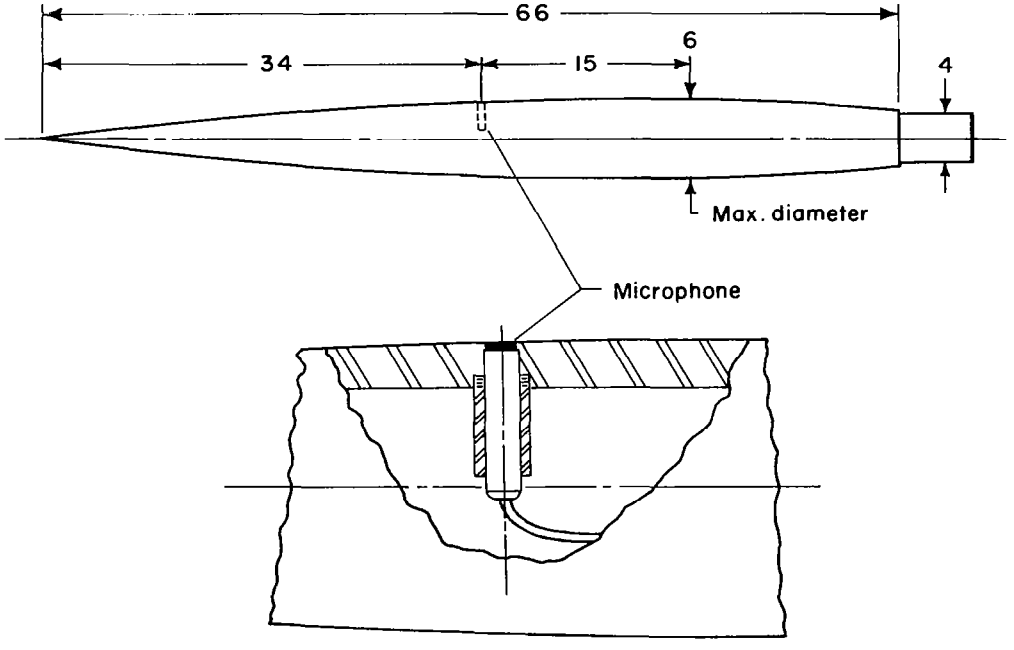

(b) Static-orifice microphone mounting.

Figure 3.- The two configurations used in sting-mounting the Altec condenser microphone in the test section.

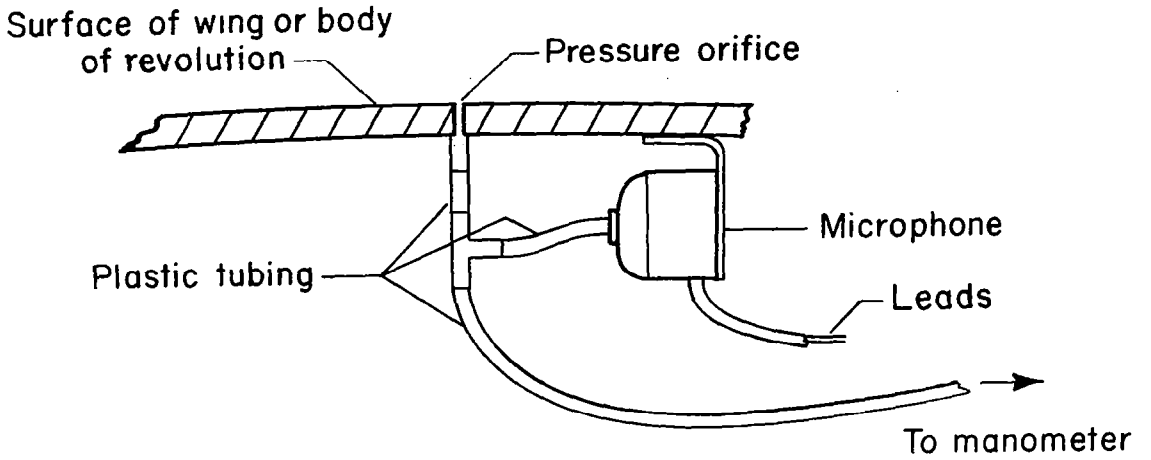

(a) Internal microphone installation for bodies of revolution and wing.

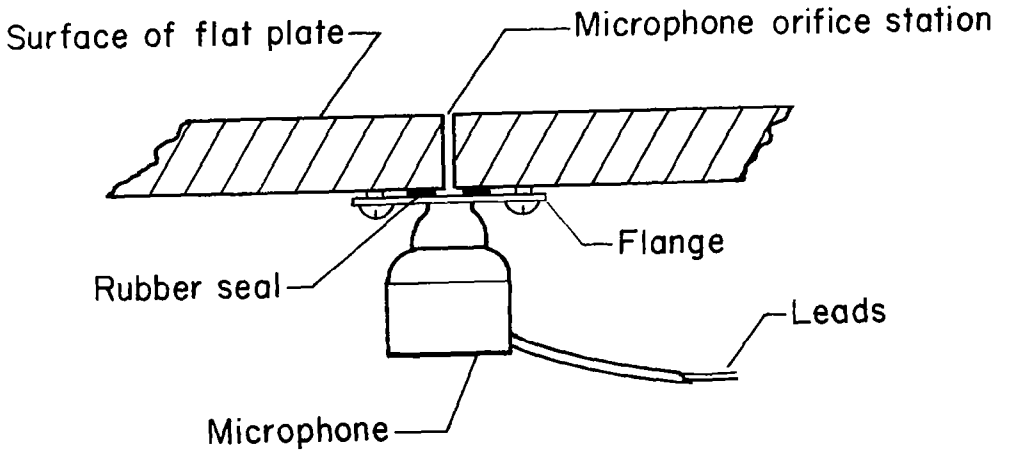

(b) Microphone installation for flat plate.

Figure 4.- The instruments used to detect transition in the boundary layer.

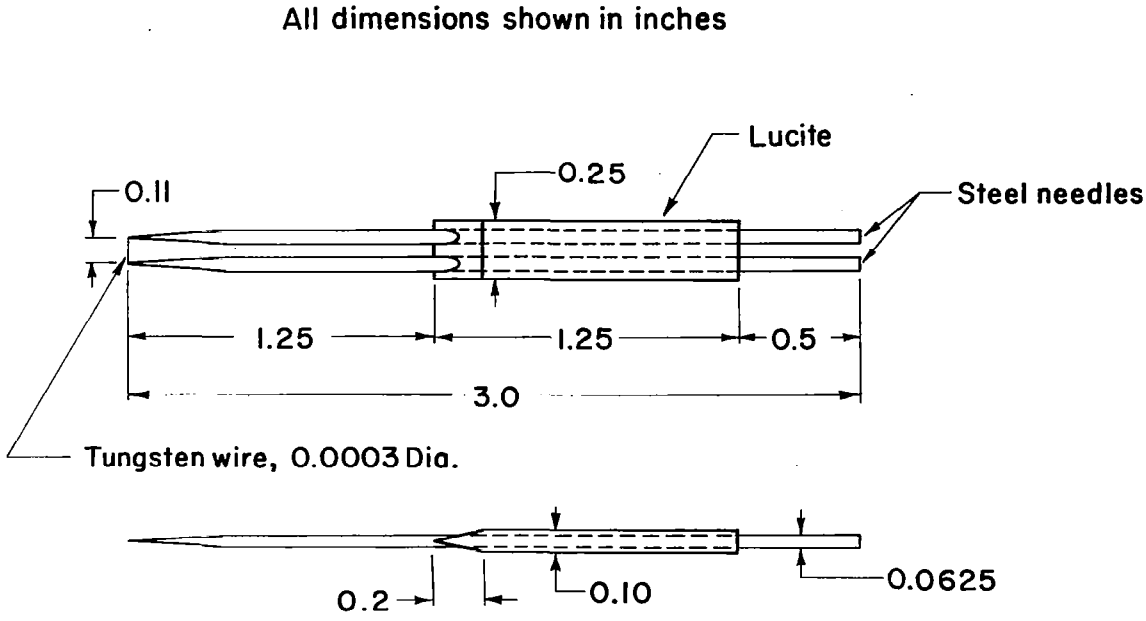

(c) Surface-mounted hot-wire probe used on the wing and the flat plate.

Figure 4.- Concluded.

(a) Laminar boundary layer.

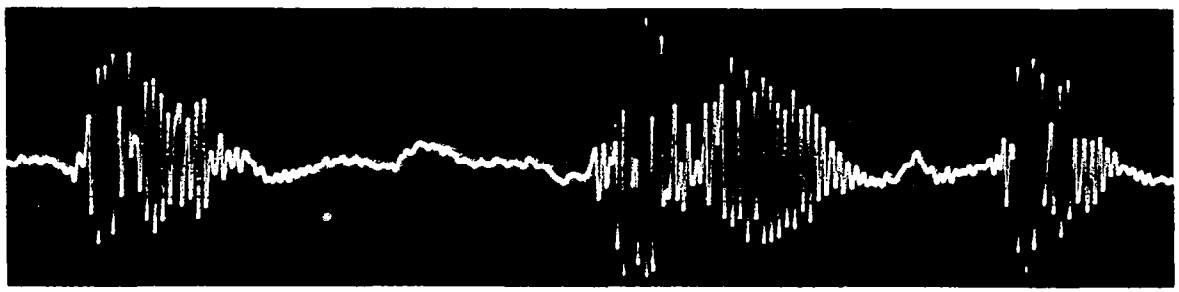

(b) Transitional boundary layer.

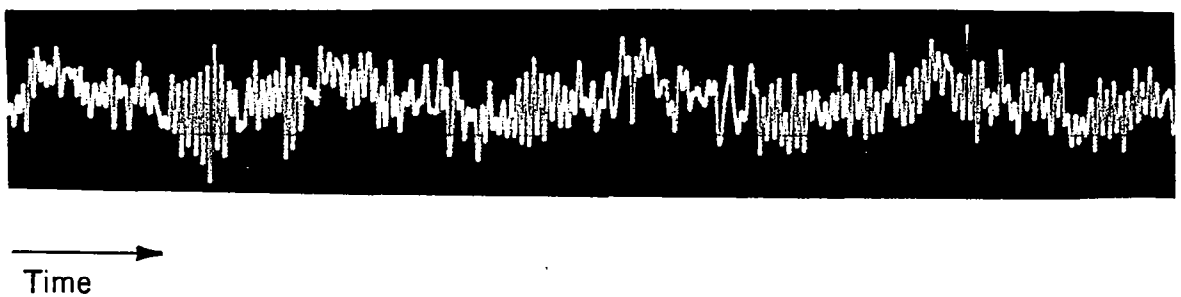

(c) Turbulent boundary layer.

Figure 5.- Representative oscilloscope traces of the hot-wire and microphone response to the three types of boundary layers.

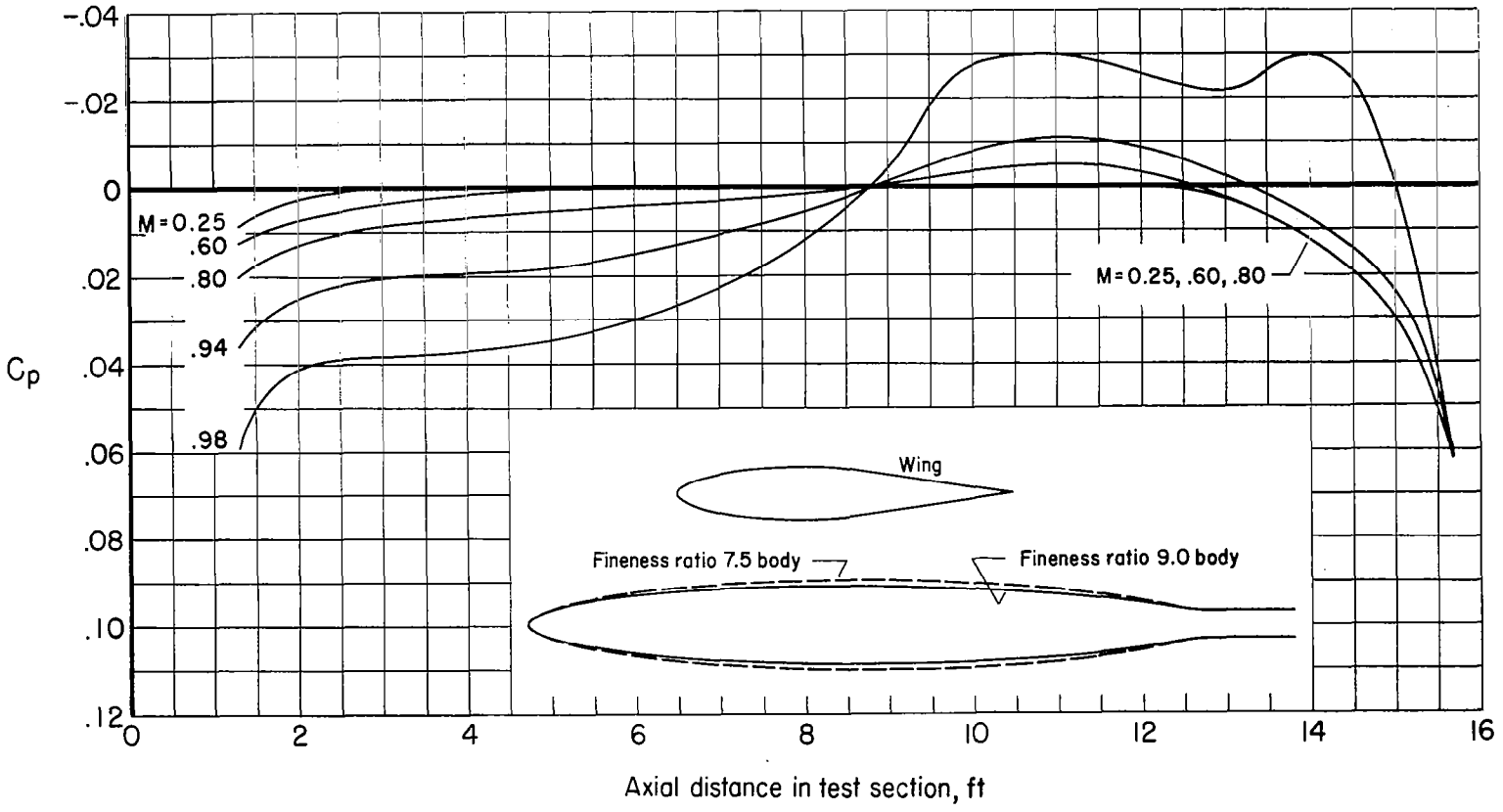

Figure 6.- The variation of static-pressure coefficient through the test section with the tunnel empty.

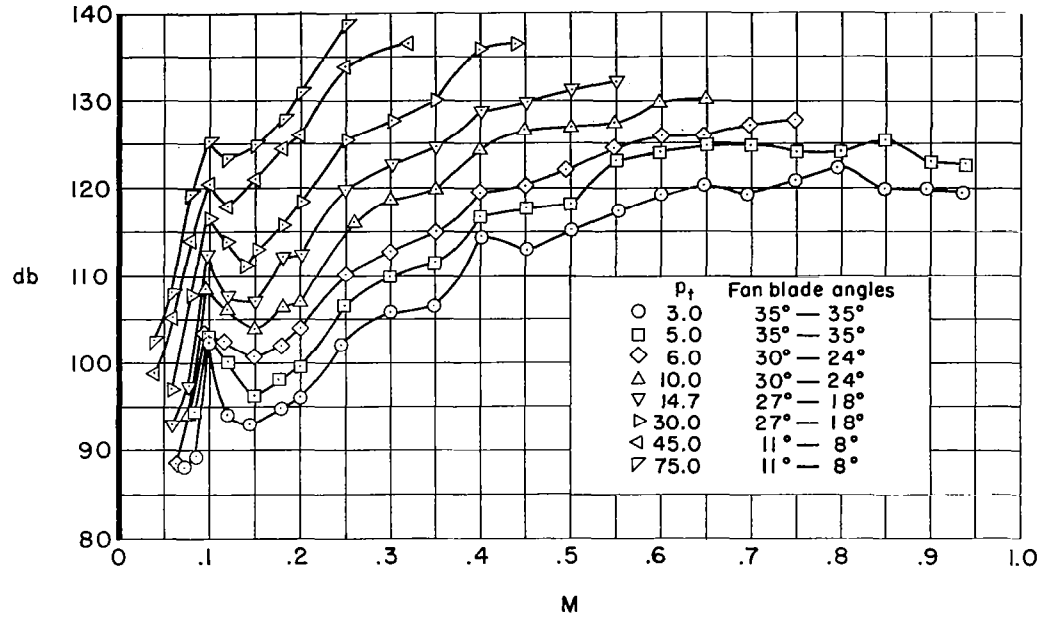

(a) Stagnation-point microphone mounting.

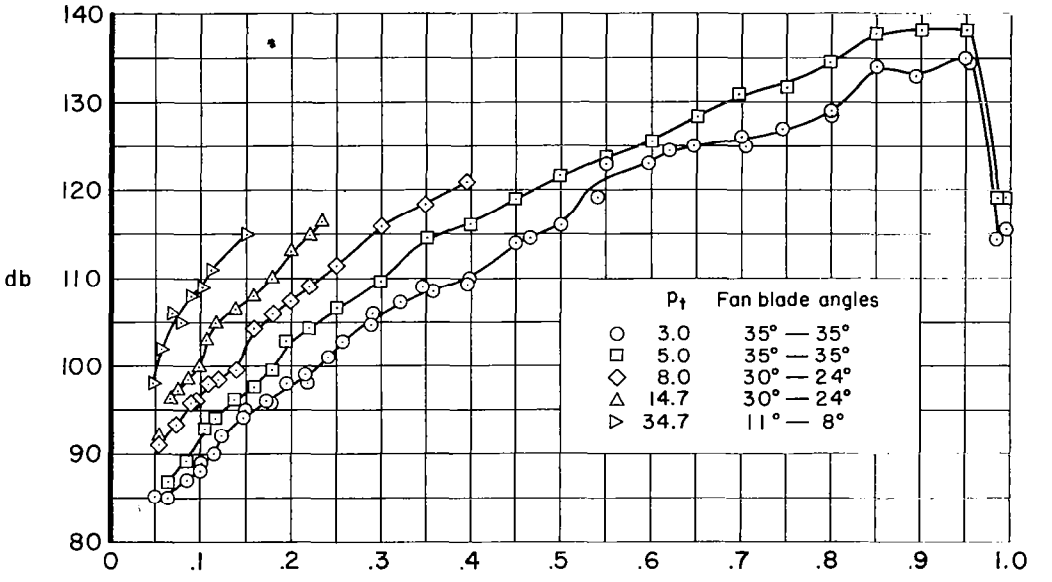

7

(b) Static-orifice microphone mounting.

Figure 7.- The variation with Mach number of the sound pressure level in the test section at several values of stagnation pressure as measured with an Altec condenser microphone supported in two different configurations.

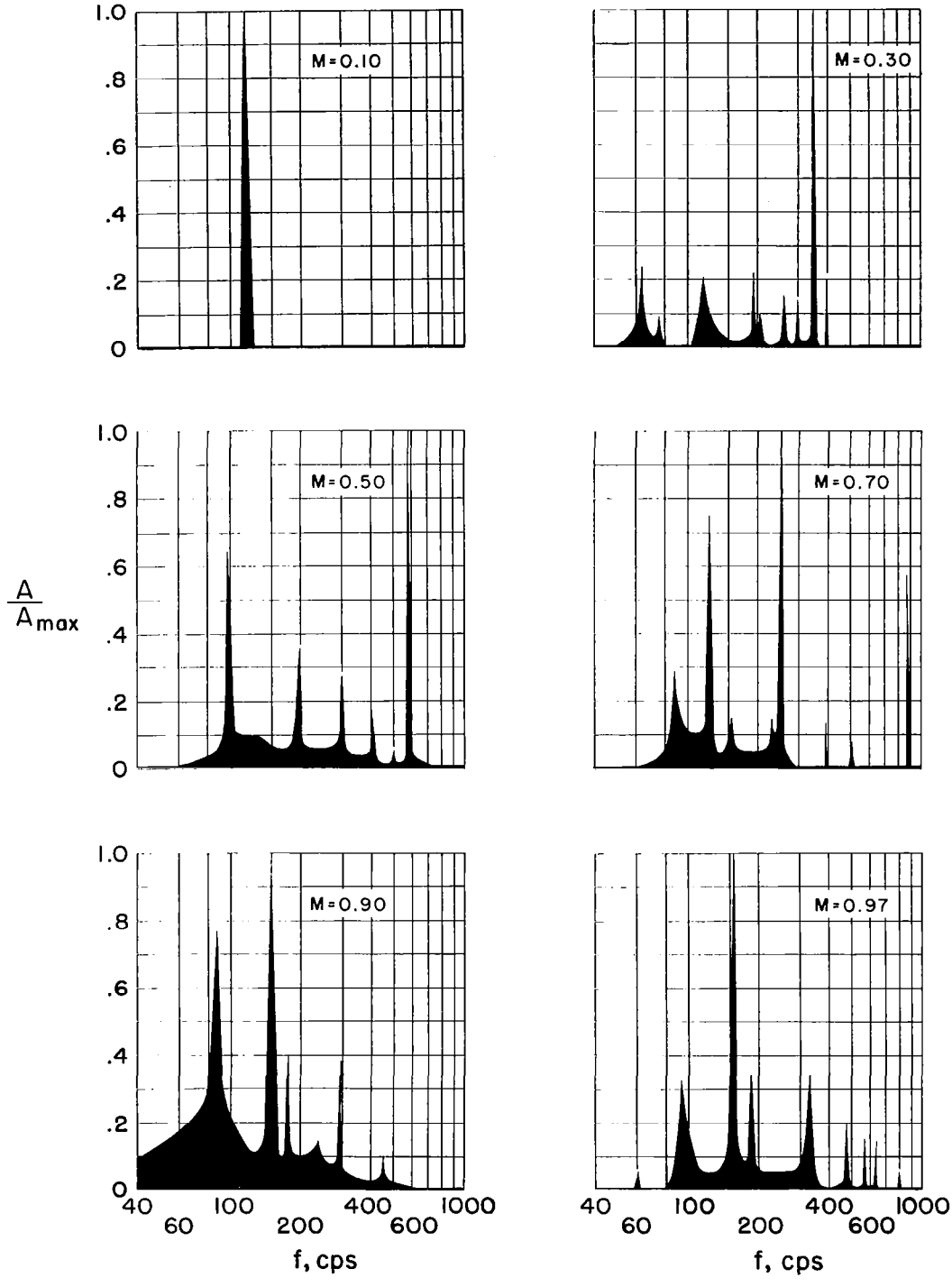

Figure 8.- The frequency spectra of sound for several Mach numbers at a stagnation pressure of 3.0 pounds per square inch.

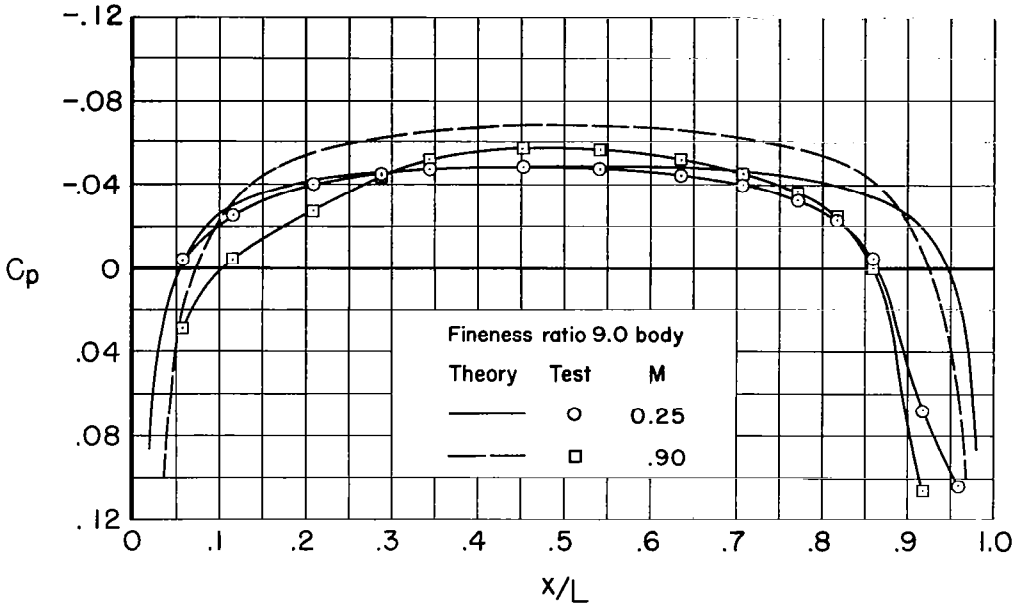

(a) Comparison between experiment and theory.

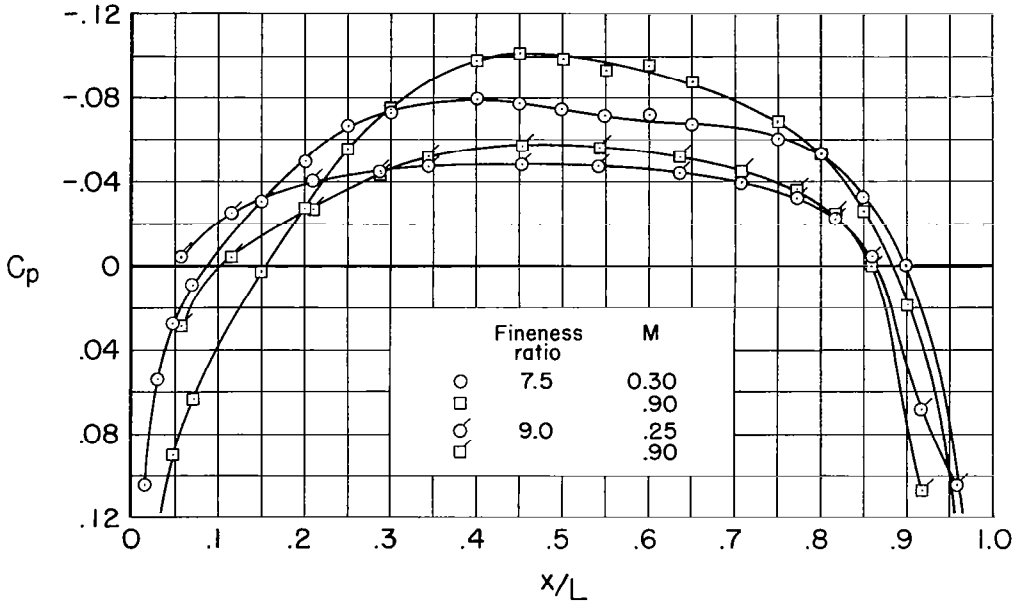

(b) Comparison between two bodies of revolution.

Figure 9.- A comparison of the distributions of pressure coefficient along the two bodies of revolution at low speed and at high speed.

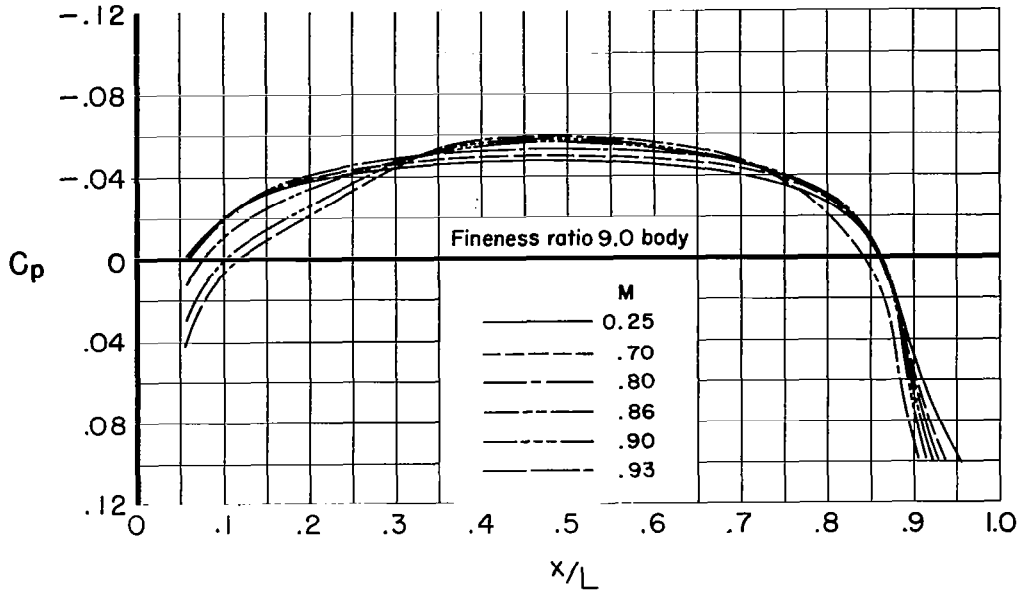

(a) Fineness-ratio-9.0 body.

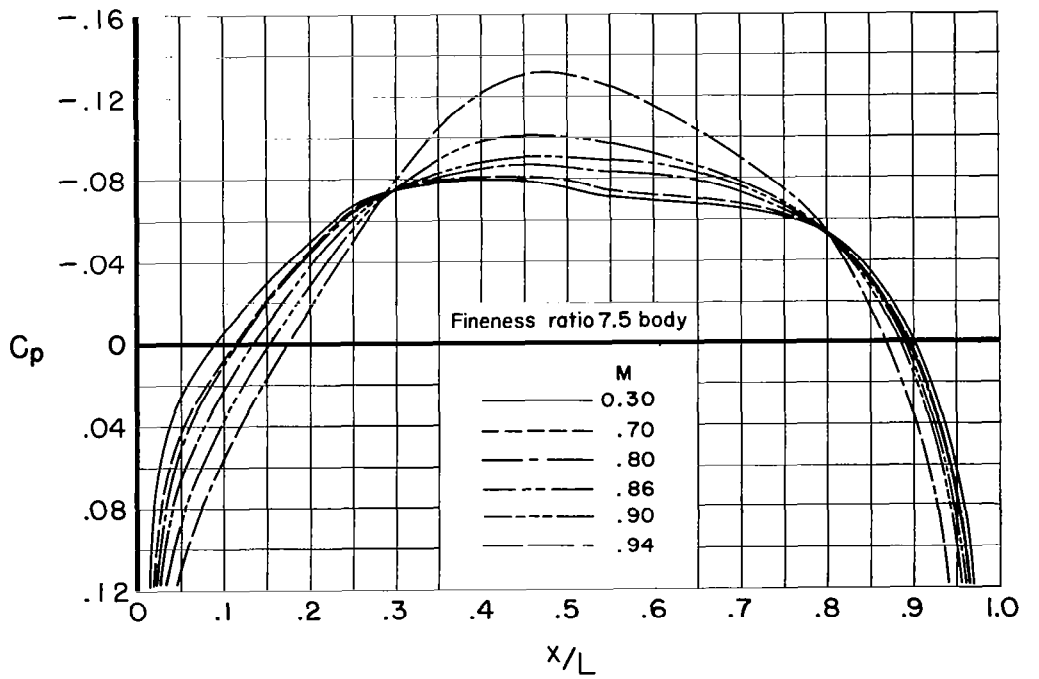

(b) Fineness-ratio-7.5 body.

Figure 10.- The distribution of pressure coefficients along the two bodies of revolution at several Mach numbers.

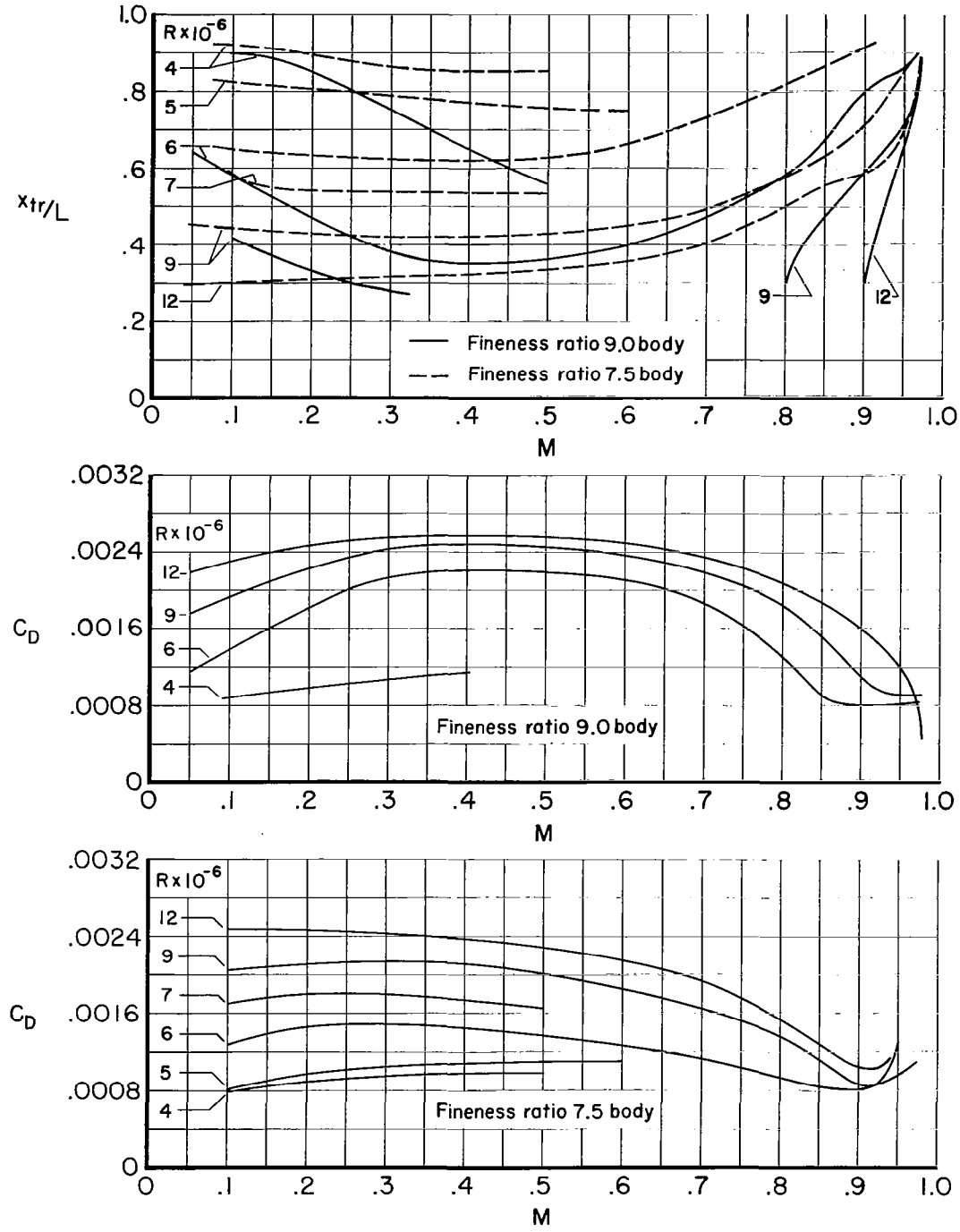

Figure 11.- The variation with Mach number of the location of transition and the drag coefficients of the two bodies of revolution at several values of Reynolds number.

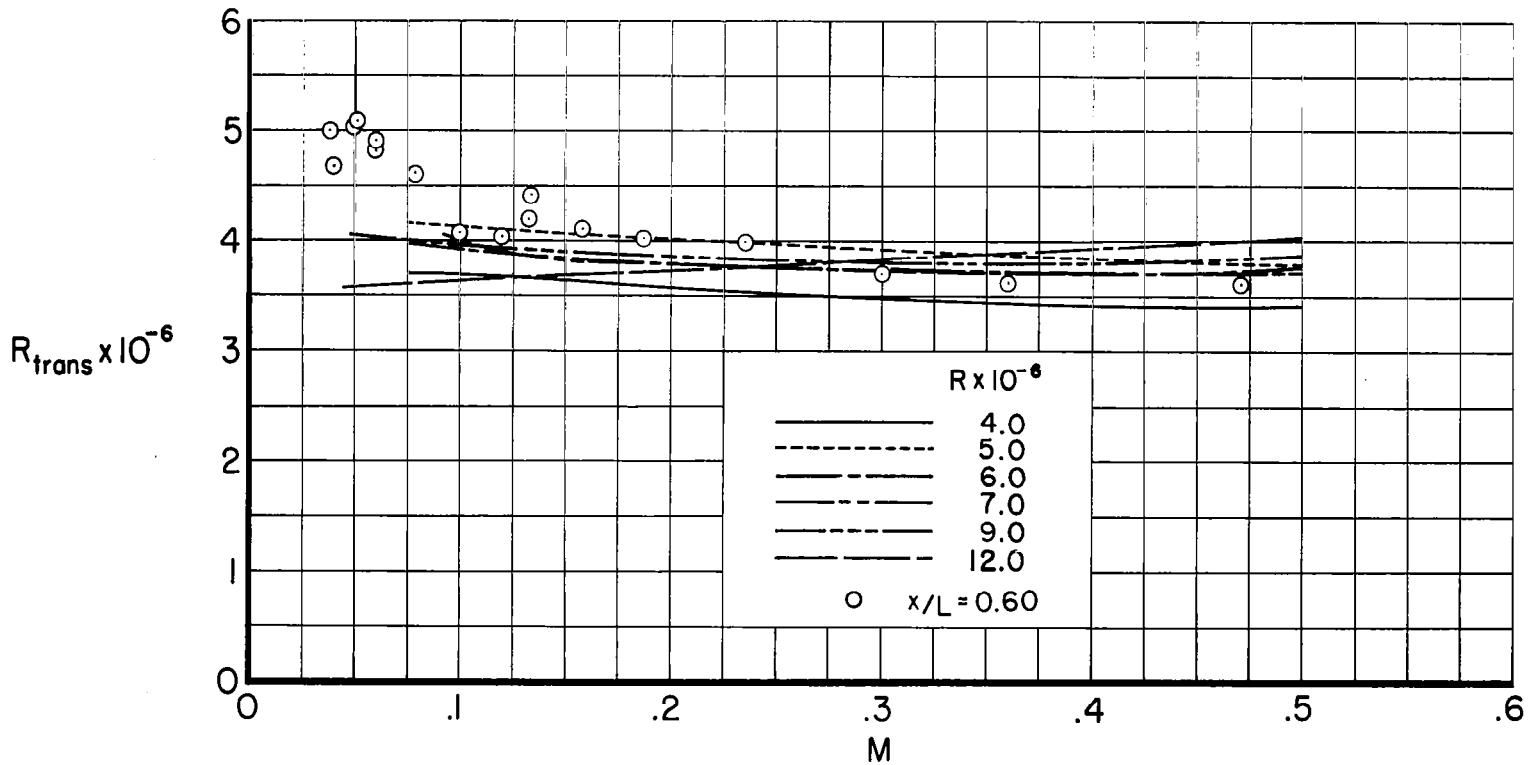

Figure 12.- The variation of transition Reynolds number with Mach number for several values of length Reynolds number and for a constant location of transition on the fineness-ratio-7.5 body.

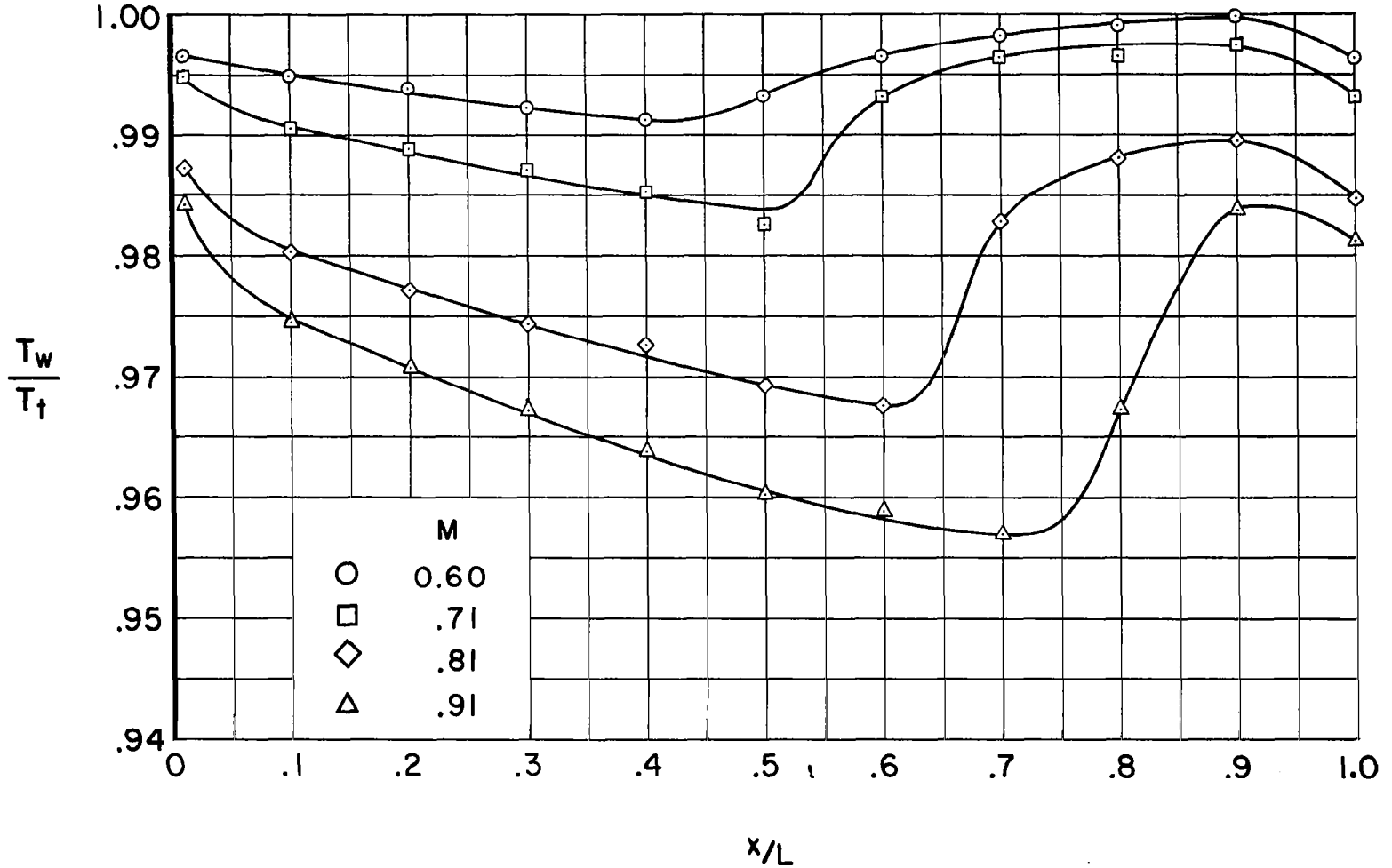

Figure 13.- The distribution of the ratio of model surface temperature to stagnation temperature along the fineness-ratio-7.5 body at a Reynolds number of 9 million for several Mach numbers.

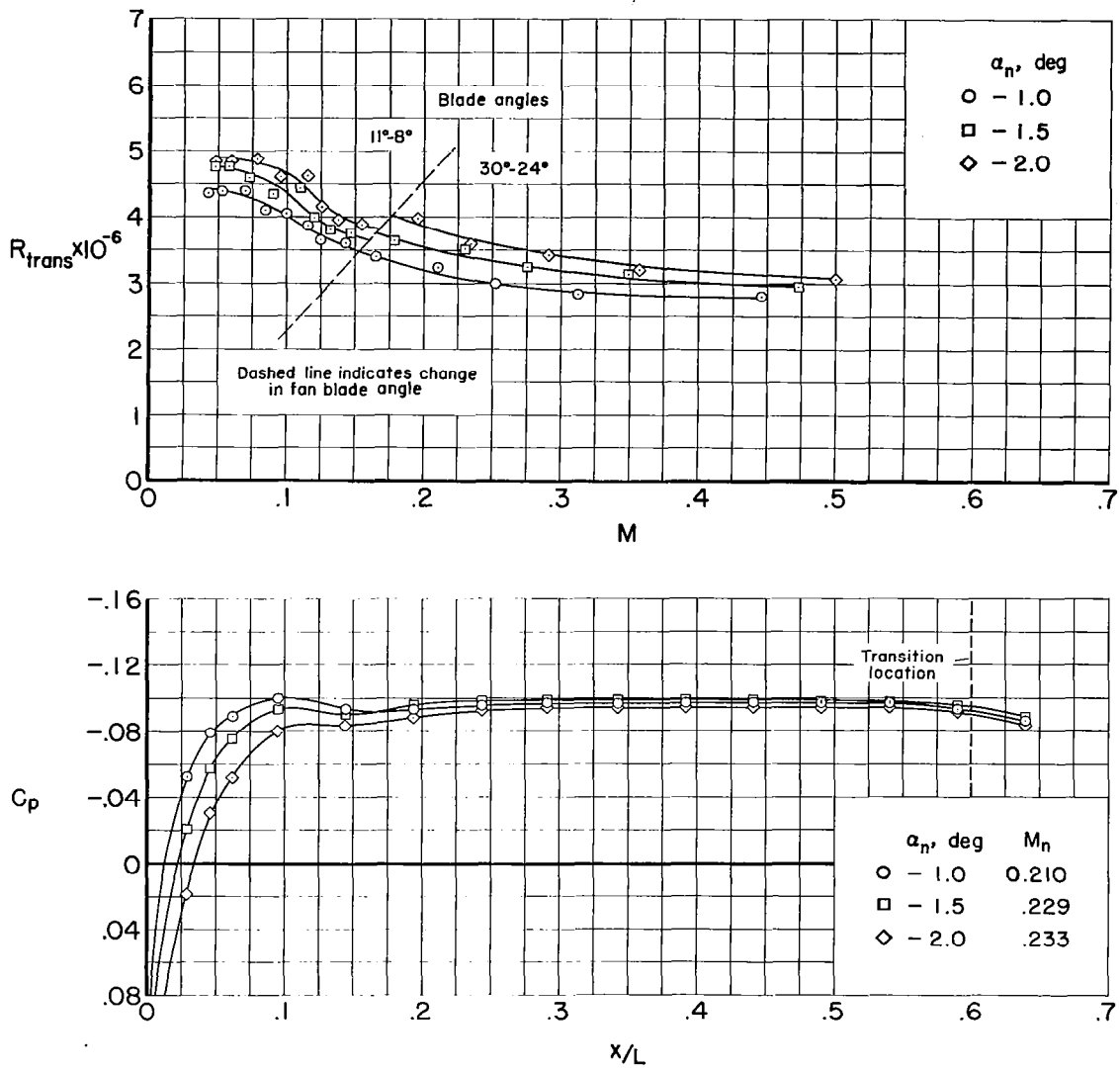

(a) $\beta = -0.18^{\circ}$

Figure 14.- The variation of transition Reynolds number with Mach number and the distribution of pressure coefficients on the flat plate for several angles of attack and three angles of channel convergence.

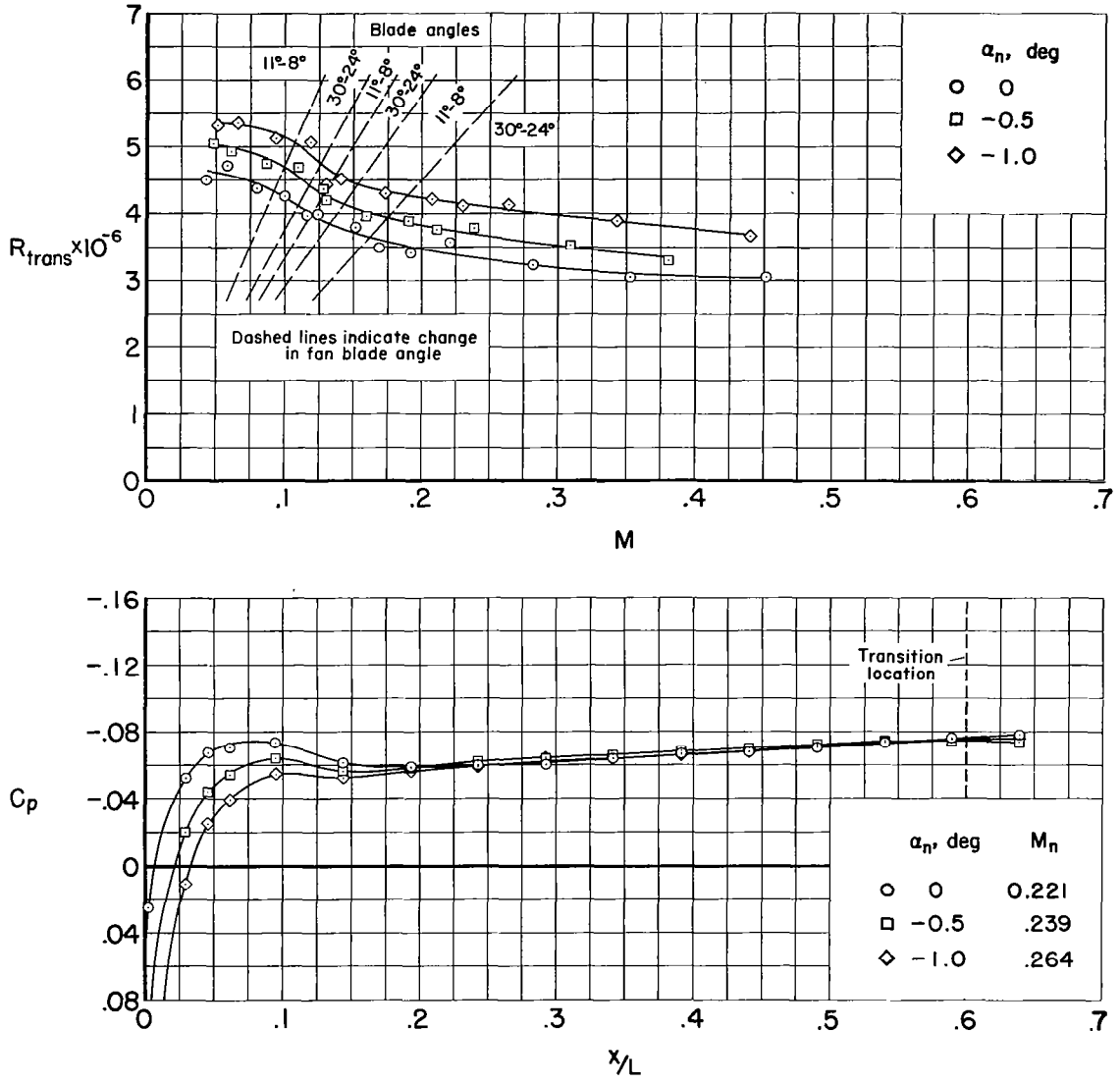

(b) $\beta = 0^\circ$

Figure 14.- Continued.

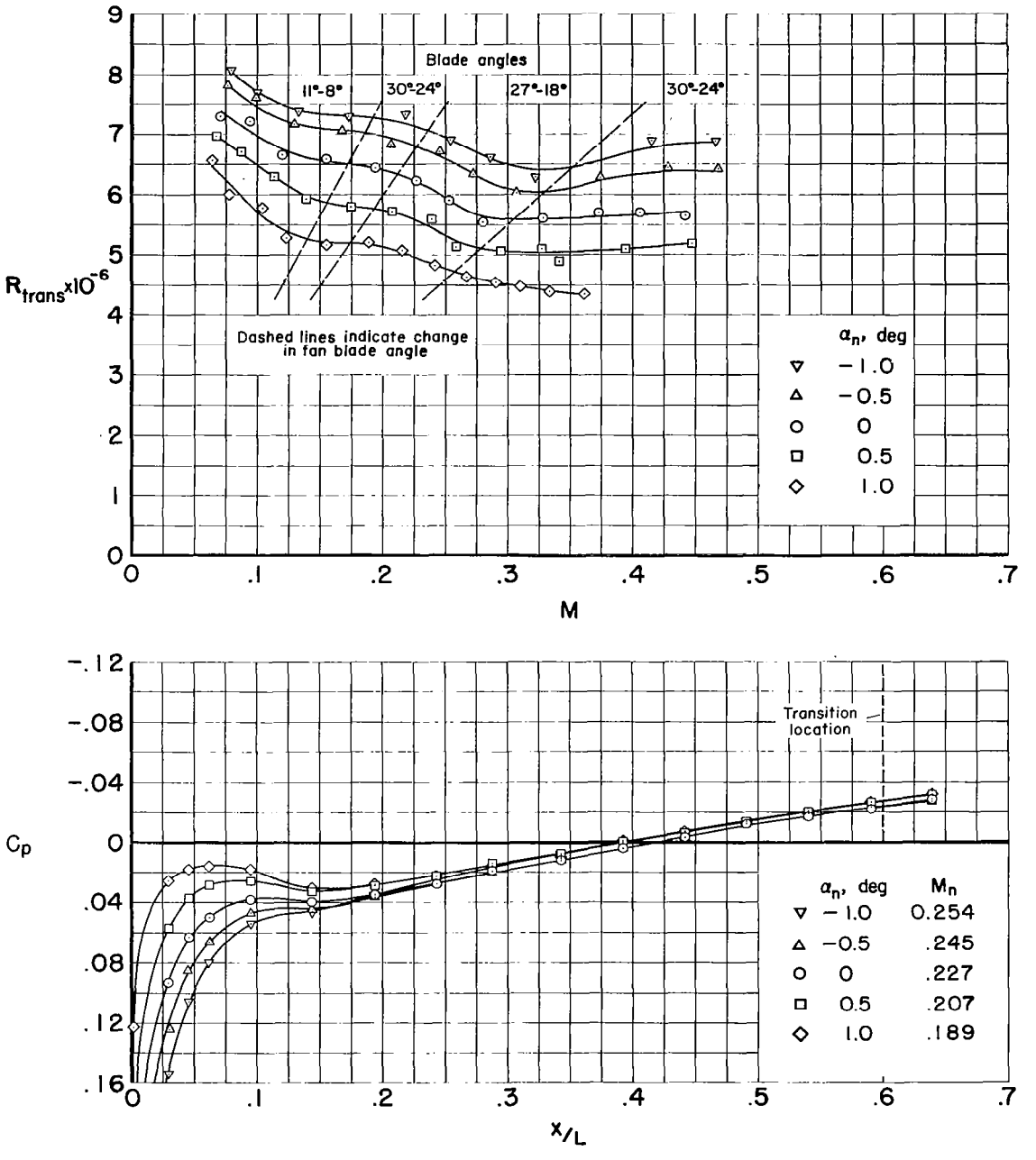

(c) $\beta = 0.60^{\circ}$

Figure 14.- Concluded.

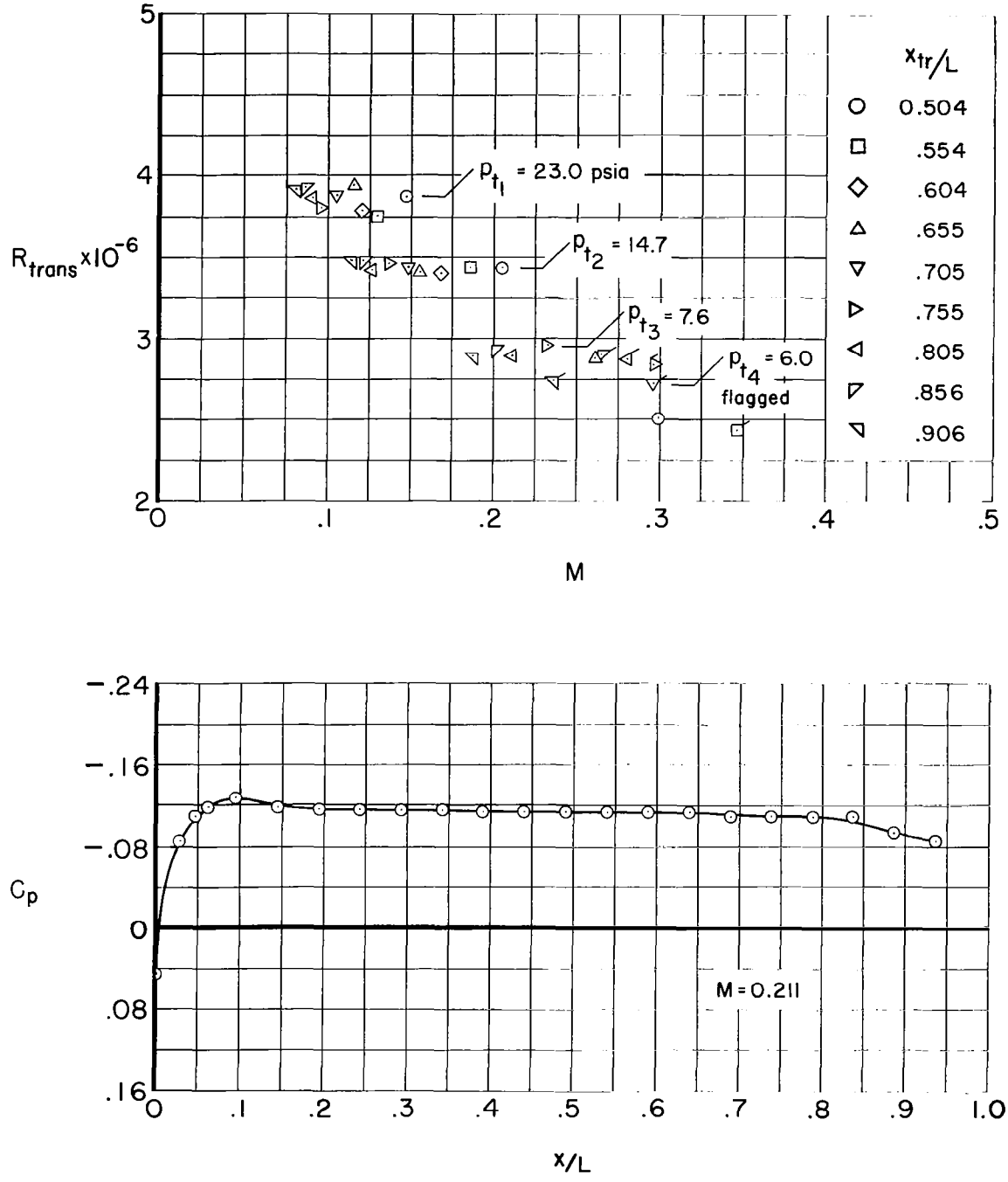

Figure 15.- The variation of transition Reynolds number with Mach number at several positions on the flat plate and a representative distribution of pressure coefficient.

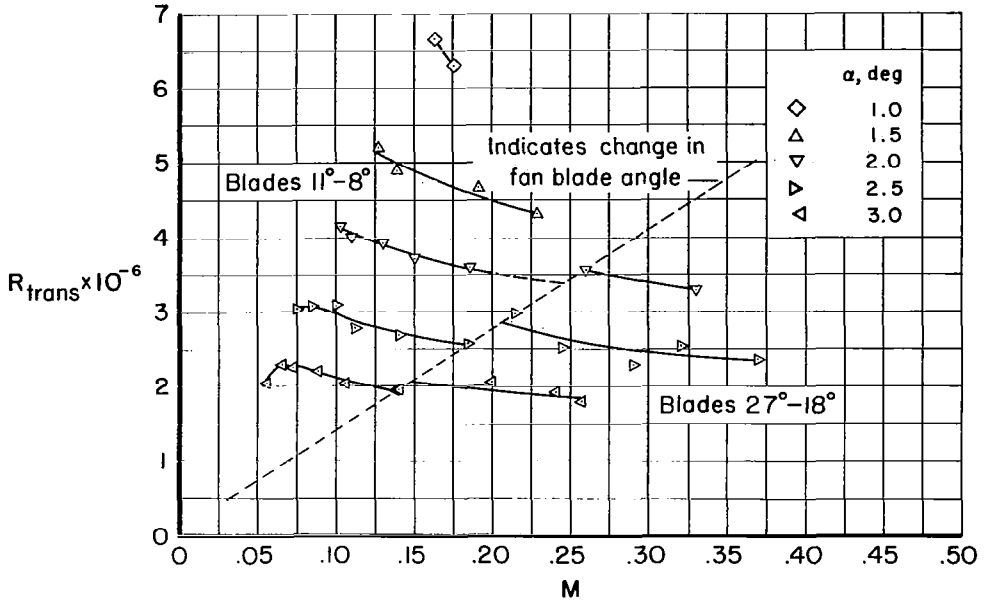

(a) $(x/c)_{tr} = 0.30$

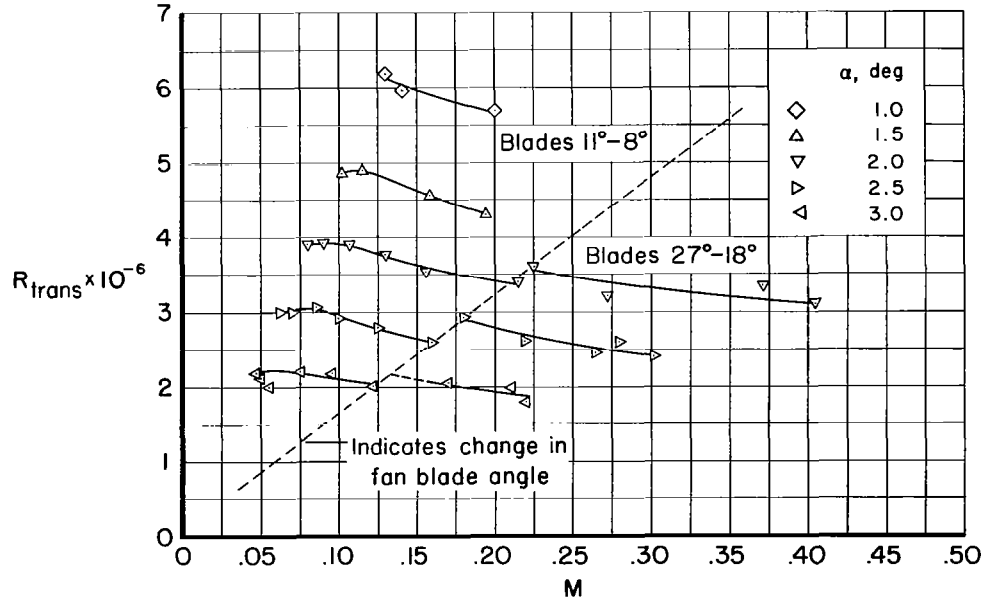

(b) $(x/c)_{tr} = 0.35$

Figure 16.- The variation of transition Reynolds number with Mach number at four chordwise positions on the wing for several angles of attack.

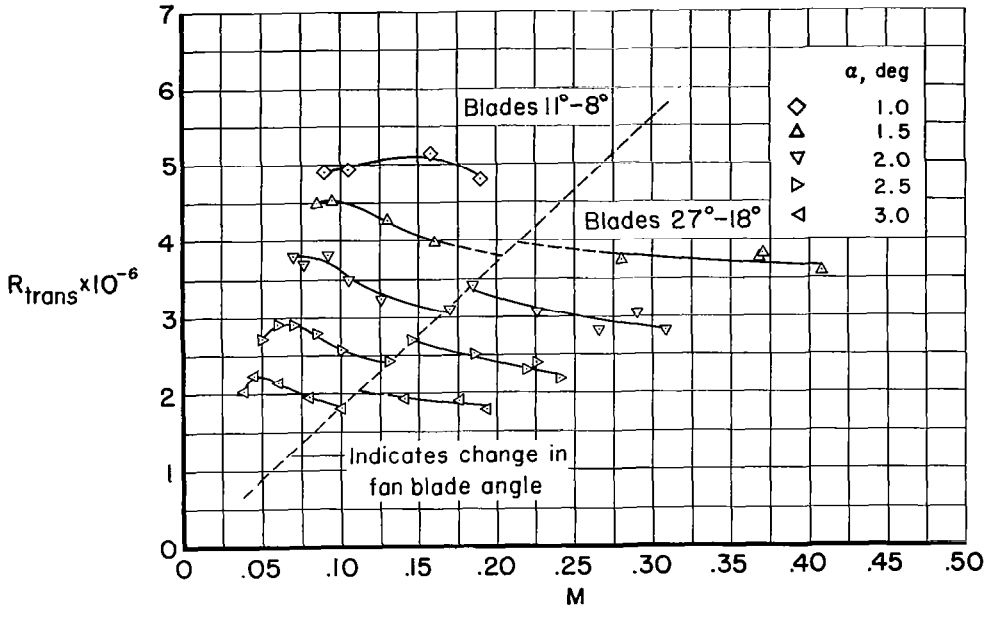

(c) $(x/c)_{tr} = 0.40$

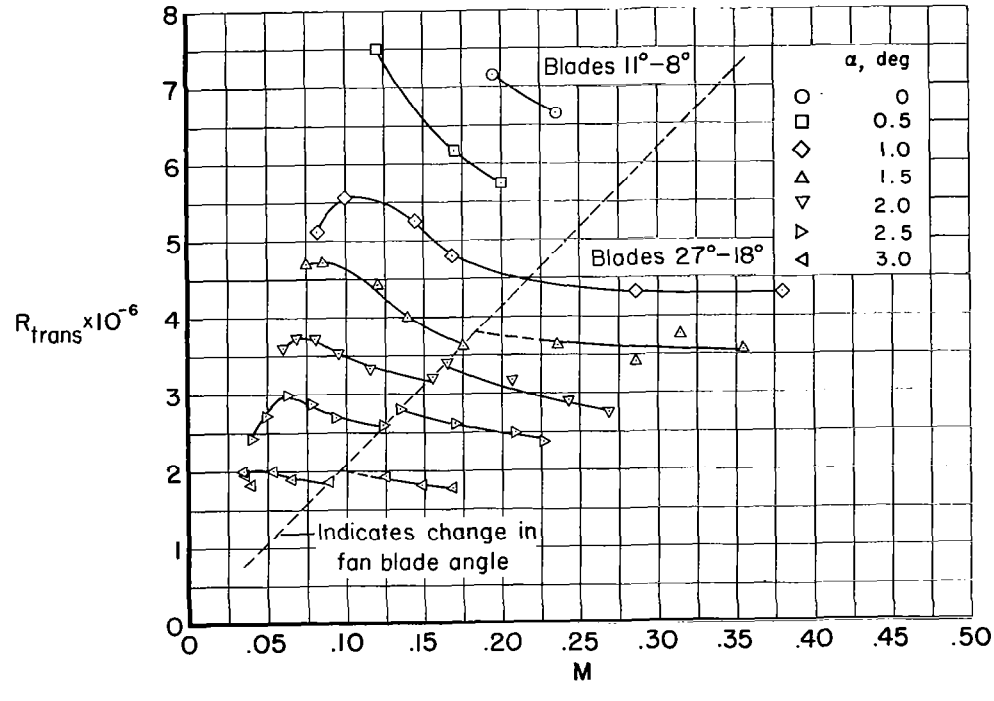

(d) $(x/c)_{tr} = 0.45$

Figure 16.- Concluded.

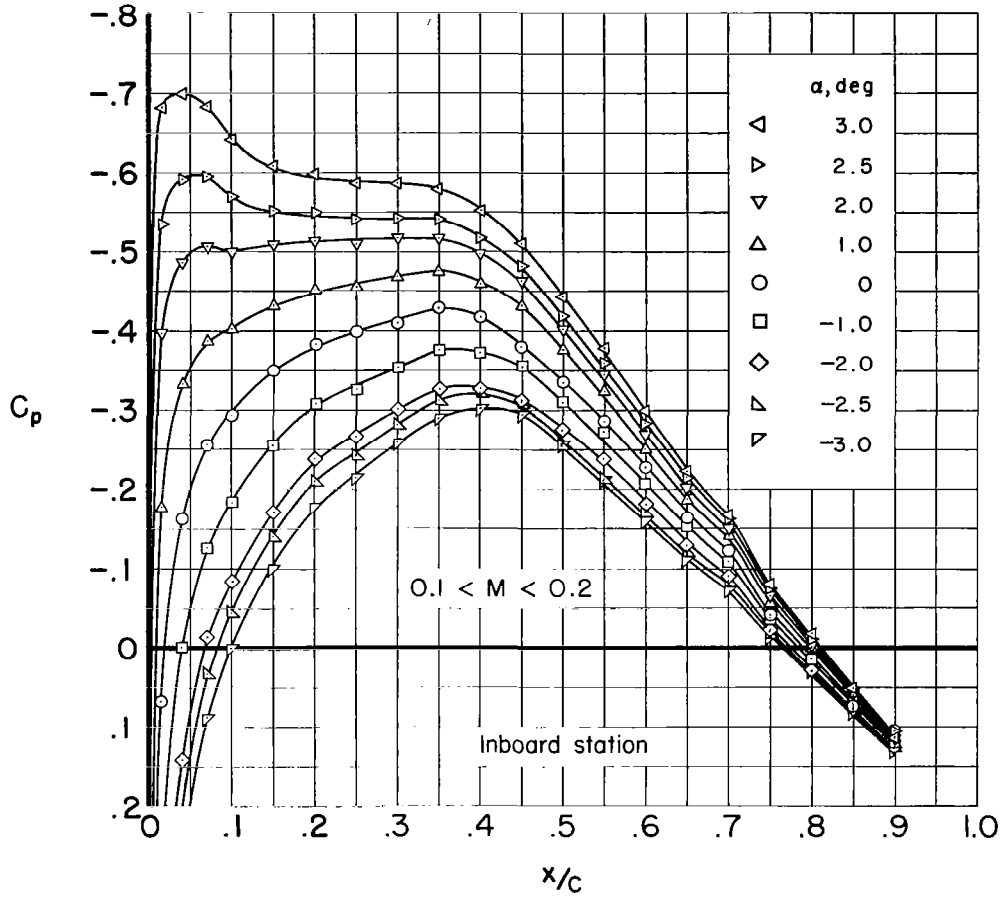

(a) $\frac{y}{b/2} = 0.45$

Figure 17.- The chordwise distribution of pressure coefficients at two spanwise stations of the wing for several angles of attack.

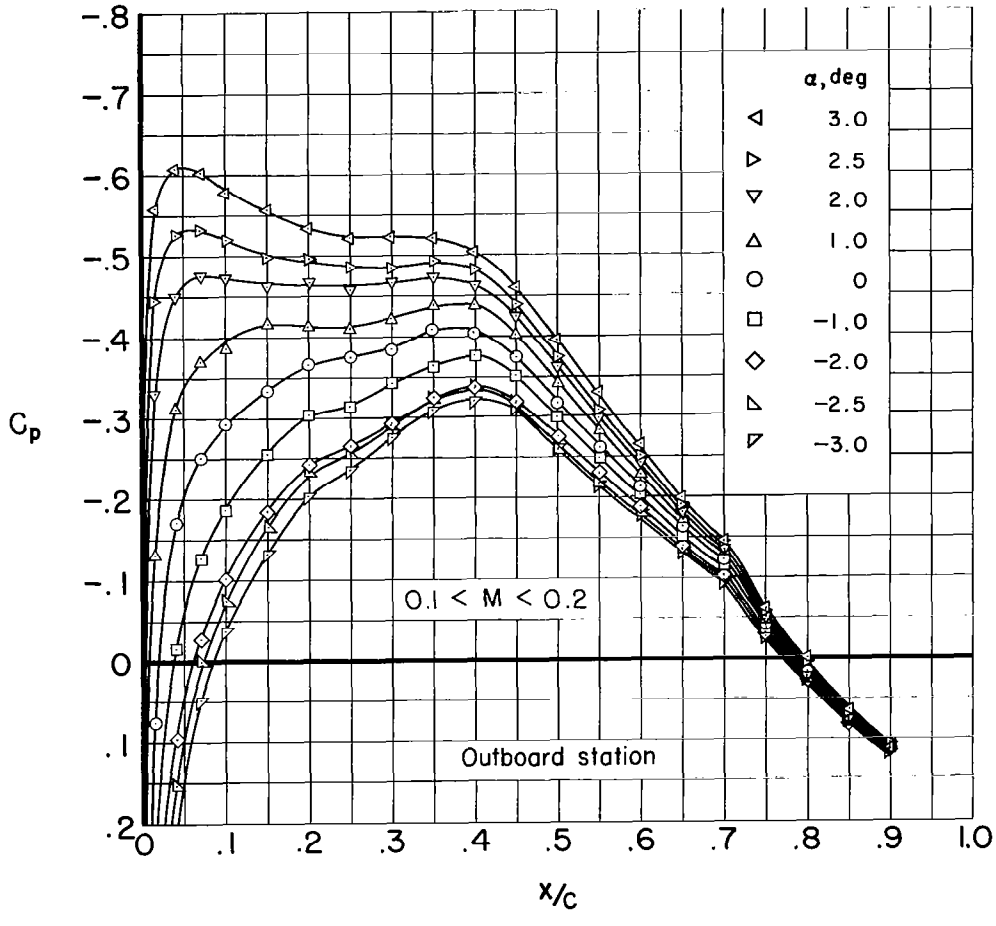

(b) $\frac{y}{b/2} = 0.80$

Figure 17.- Concluded.

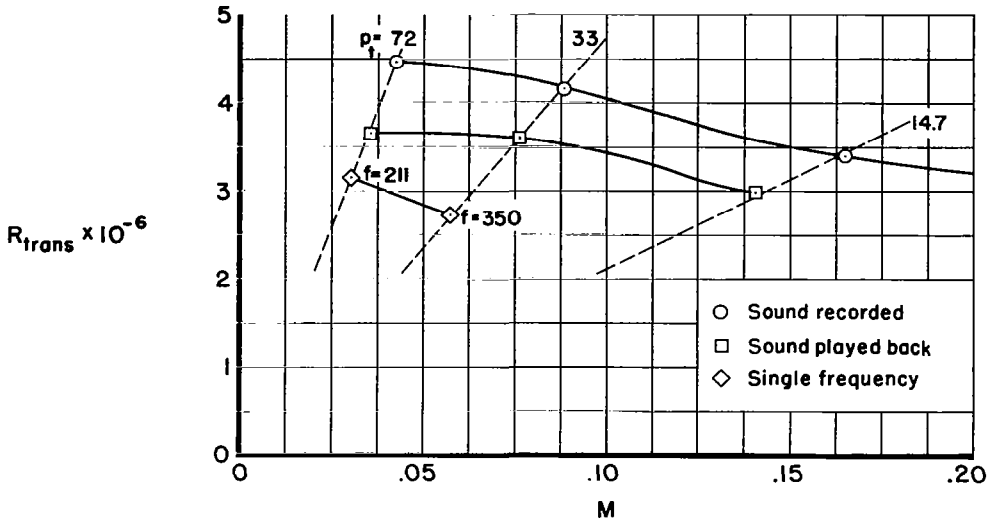

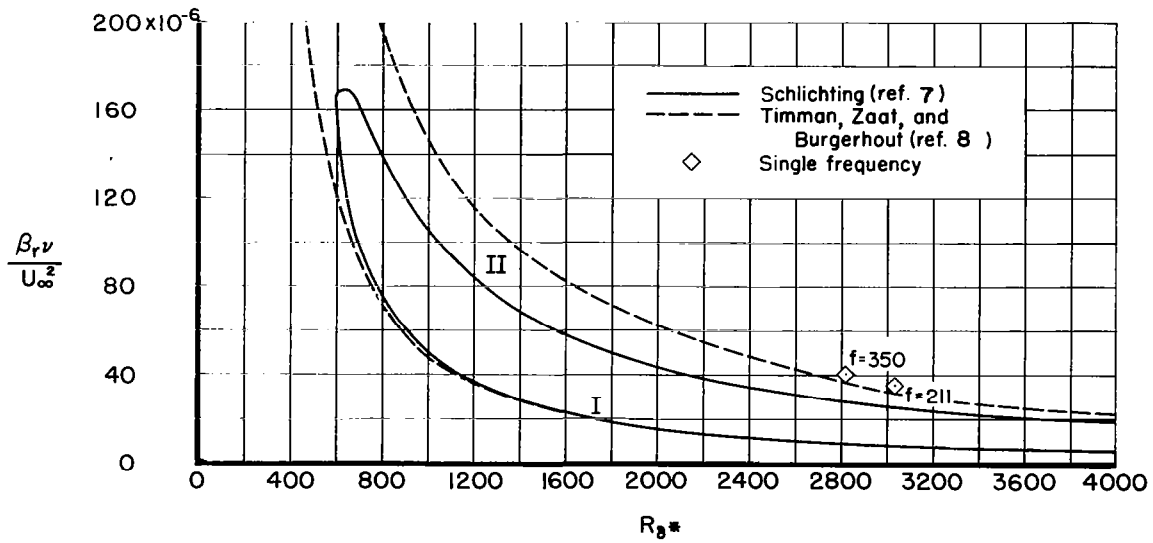

Figure 18.- The effects of artificial sound on the transition Reynolds numbers of the flat plate, and the location on the boundary-layer stability diagram of the experimental data for beginning transition as induced by single-frequency sound.

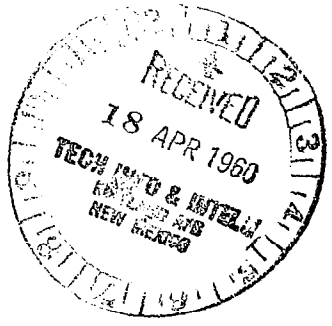
RECEIVED
18 APR 1960
TECH INFO & INTELL